ELSEVIER

Journal of Nuclear Materials 305 (2002) 134–152

journal of nuclear materials

www.elsevier.com/locate/jnucmat

Construction of radiation-modified phase diagrams under cascade-producing irradiation: application to Zr–Nb alloy

Anatole A. Turkin *, Alexander V. Buts, Alexander S. Bakai

National Science Center, Kharkov Institute of Physics and Technology, Akademicheskaya str. 1, 61108 Kharkov, Ukraine

Received 18 October 1999; accepted 26 June 2002

Abstract

A general theoretical formalism developed for the description of phase stability alteration in substitutional binary alloys under irradiation is applied to Zr–Nb alloys. We examine the stability of β-Nb precipitates in Zr–Nb alloy subjected to the cascade-producing irradiation. The results of phase stability studies are presented in the form of radiation-modified phase diagram. Evolution of large precipitates (as compared to the size of cascade region) differs from that of small precipitates. In the radiation-modified phase diagram there exists a low temperature boundary for stability of large precipitates, the location of which depends on interface type and displacement rate. Above this boundary large precipitates coarsen with radiation-enhanced rate. Below it the alloy is maintained in a quasi-steady-state of supersaturated solid solution with a population of fine-grained precipitates. The competition between processes of cascade destruction; nucleation and growth of coherent precipitates; and coherency loss can lead to the formation of the distribution of fine-grained precipitates with slowly varying parameters. In particular, such a distribution may form in Zr–Nb alloys under thermal reactor conditions.

PACS: 61.80.Az; 61.82.Bg; 81.30.Bx

1. Introduction

The majority of modern commercial multicomponent alloys are fabricated and used in a metastable state. The alloy may contain precipitates of non-equilibrium phases and/or phases supersaturated with one of components. During service at elevated temperatures the metastable phase microstructure of the alloy evolves toward the thermally equilibrium state that can be predicted using the alloy phase diagram. The time to reach this equilibrium state (or the lifetime of the initial phase microstructure) depends on temperature and external dynamical forcing such as irradiation in nuclear reactors. Usually, without irradiation this time is large as compared to human time scales (otherwise the material has no or little value). Irradiation of multicomponent alloys by energetic particles often leads to dramatic changes in their phase microstructure. Sometimes the standard phase diagram can be used for predicting microstructural phase changes induced by irradiation. Obviously, because of enhancement of atomic mobility, irradiation accelerates nucleation and growth of phases, which are formed under thermal conditions.

However, in reality irradiation affects phase stability in a more complicated way – precipitation of non-equilibrium phases, or conversely, dissolution of thermally stable precipitates existing prior to irradiation are frequently observed (for reviews and discussions see

* Corresponding author. Tel.: +380-572 356 203; fax: +380-572 352 683.

E-mail address: anatole.turkin@kipt.kharkov.ua (A.A. Turkin).

0022-3115/02/$ - see front matter
PII: S0022-3115(02)01027-9

Refs. [1–5]). To forecast the behavior of the alloy under irradiation, one needs a method to construct a radiation-modified phase diagram – an analog of the phase diagram that would contain the 'equilibrium' diagram as a limiting case required for experimental verification. It would be desirable to formulate an approach allowing for the prediction, as a function of the forcing conditions, of possible steady-states of such systems, of the respective stability of the various a priori possible states, as well as of the evolution path to that state. In the absence of external influences, similar questions deal with thermal equilibrium states and are addressed by equilibrium and irreversible thermodynamics. The latter provides the necessary background for construction of a more general formalism for descriptions of driven systems far away from equilibrium. An evident reason is that the equilibrium properties of materials influence their behavior under non-equilibrium conditions.

Irradiation strongly affects the evolution of phase composition of alloys. During past decades the basic physical mechanisms, which are responsible for phase stability loss under irradiation, have been identified [1–5]. These mechanisms include radiation mixing, radiation-enhanced diffusion and radiation-induced segregation. Both radiation mixing and disordering are most pronounced when the alloy is subjected to cascade-producing irradiation. The radiation-induced mixing contributes to the redistribution of atoms at low temperatures when the thermal atomic mobility is frozen [6,7]. The radiation-enhanced diffusion is controlled by migration of non-equilibrium point defects (PD), vacancies and interstitial atoms, which are created by irradiation. The radiation-induced segregation – the change of the alloy composition in the vicinity of PD sinks – is caused by the coupling of PD fluxes with the fluxes of alloying elements (the inverse Kirkendall effect [8]). The spatial inhomogeneity of mutual recombination of PD (for example, at the coherent boundary containing traps for PD [9] or in the bulk of coherent precipitates [10]) may also result in segregation, and therefore affects the processes of nucleation and growth of precipitates.

Phase stability loss is explained in the literature as a result of action of one or several mechanisms simultaneously. For example, a large body of experimental data shows that the competing kinetics of the processes of cascade mixing and radiation-enhanced diffusion leads to the appearance of a low temperature threshold for stability of second phase precipitates in alloys under irradiation (see Refs. [4,11,12]). This effect – the combined influence of radiation-induced segregation and cascades mixing on the stability of large (as compared with a cascade size) coherent and incoherent precipitates in a disordered substitutional alloy – we studied in Refs. [13–15]. The results were presented in the form of radiation-modified phase diagram.

The purpose of this paper is to apply to the particular case of the Zr–Nb alloy the general formalism developed in Refs. [14,15] for the description of phase stability alteration under irradiation. In this paper we consider the stability of β-Nb precipitates in the α-Zr matrix under irradiation. It is known that below the monotectoid temperature the thermally stable state of a binary Zr-alloy with a few percent of Nb is the solid solution of Nb in the α-Zr matrix containing precipitates of the β-Nb phase. The boundary of the two-phase field in the Zr corner of the phase diagram is the thermal solvus of Nb in the α-Zr phase.

According to experimental data, irradiation enhances decomposition of metastable supersaturated solid solutions of Nb in the α-Zr matrix resulting in precipitation of β-Nb particles (see Section 3). Moreover, under prolonged irradiation one might expect a decomposition of the β-Zr phase that can be present in the Zr–Nb alloy quenched from the α-Zr + β-Zr state. Thus, intuitively, it seems that the quasi-steady-state, which the Zr–Nb alloy reaches after high dose irradiation, is again, as in the thermal case, the α-Zr matrix with precipitates of the β-Nb phase and Nb atoms in solid solution. However, it is clear that the shape of the two-phase field should differ from that given by equilibrium phase diagram. One obvious reason is that at sufficiently low temperatures cascades destroy precipitates that grow by diffusion-limited kinetics (enhanced by irradiation). This means that at low temperatures cascade-producing irradiation maintains the solid solution in a supersaturated state and does not allow precipitates to grow to large sizes. Another important point is that radiation-induced segregation influence stability of incoherent precipitates, which are sinks for PDs. Therefore the shape of stability regions of precipitates may depend on their interface type.

The goal of this paper is to find how irradiation influences the location of boundaries of two-phase field α-Zr + β-Nb in the Zr corner of the phase diagram. In other words, we want to reveal factors, which influence the stability of β-Nb precipitates, and to find is it possible to define a radiation-modified solubility.

Our logic is as follows: if a 'test' precipitate embedded into solid solution is unstable under irradiation it will never form in the irradiated alloy with the same solid solution concentration. The growth rate of the precipitate is controlled by the solute concentration in the solution. If, under thermal conditions, the solute concentration equals the solubility limit then the precipitate growth rate is zero. The precipitate dissolves if the solute concentration is less than the solubility limit. Under irradiation the situation is similar – there exists a solute concentration at which the precipitate growth rate is zero. This concentration depends on irradiation conditions and separates regions of negative and positive precipitate growth rates. By analogy with the thermal

case we call it the radiation-modified solubility. The radiation-modified solubility depends on type of irradiation and kinetics of PD at precipitate interfaces, i.e. on interface type. In the phase diagram the temperature dependence of coherent and incoherent radiation-modified solubilities bound the fields of stability of respective precipitates. Thus, we have the radiation-modified diagram. Ultimately, the irradiated alloy will evolve to one of the quasi-steady-states given by the radiation-modified phase diagram.

In this paper we do not consider the evolution of the β-Zr phase under irradiation. One cannot rule out that the β-Zr phase can influence nucleation and growth of β-Nb precipitates in the α-Zr matrix. Decomposition $\beta\text{-Zr} \rightarrow \cdots \rightarrow \alpha\text{-Zr} + \beta\text{-Nb}$ would increase the Nb concentration in the solid solution. Another possibility is that the radiation stabilizes the β-Zr phase (see Section 4). However, evolution of the β-Zr phase cannot influence the radiation-modified solubilities of Nb in the α-Zr matrix, which are calculated in this paper.

In Section 2 we summarize the main ideas of our approach and introduce the concept of a radiation-modified solubility. Then we discuss the experimental data on the behavior of precipitates of the β-Nb phase in the Zr–Nb alloy. Finally, we calculate the radiation-modified phase diagram of the Zr–Nb alloy both for electron and for cascade-producing irradiation.

2. The model

2.1. Diffusion equations

Here, following the previous papers [13,14], we will outline the model for solute and PD diffusion. Consider a substitutional binary alloy A–B with the concentrations C_A, C_B. ($C_A + C_B = 1$, $C_B > C_A$, where C_A is the solute in the following. Throughout the paper, the concentrations are defined in terms of atomic fractions.) The alloy may contain coherent and incoherent precipitates of an ordered phase. The solute concentration in the precipitate C_A^P is assumed to be larger than that in the matrix. In this case, the growth of the precipitate is controlled by the diffusion of the element A. Cascade-producing irradiation creates in the alloy non-equilibrium vacancies and interstitial atoms. For the sake of simplicity, we assume that these PD do not interact with stress fields that can be produced by microstructural defects. To describe the diffusion and segregation processes we use the set of equations for vacancy, interstitial and solute concentrations:

$$\frac{\partial C_{i,v}}{\partial t} = K - \alpha_R D_i C_i C_v - \operatorname{div} \mathbf{j}_{i,v}, \tag{1}$$

$$\frac{\partial C_A}{\partial t} = -\operatorname{div} \mathbf{j}_A + g(\mathbf{r}), \tag{2}$$

$$\mathbf{j}_i = -\nabla D_i C_i, \quad D_i = \frac{d_{Ai}\xi C_A}{C_B + \xi C_A} + \frac{d_{Bi} C_B}{C_B + \xi C_A}, \tag{3}$$

$$\begin{aligned} \mathbf{j}_v &= -D_v \nabla C_v + (d_{Av} - d_{Bv}) C_v \nabla C_A \\ &= -D_v^2 \nabla (C_v / D_v), \quad D_v = d_{Av} C_A + d_{Bv} C_B, \end{aligned} \tag{4}$$

$$\begin{aligned} &\mathbf{j}_A = -d_{Av} C_v \nabla C_A + d_{Av} C_A \nabla C_v - \nabla D_i C_i \frac{\lambda C_A}{C_B + \lambda C_A}, \\ &\lambda = \frac{d_{Ai}}{d_{Bi}} \xi, \end{aligned} \tag{5}$$

where C_i and C_v are the interstitial and vacancy concentrations, respectively; K is the generation rate of freely migrating PD [6]; α_R is the recombination rate constant; d_{Ai} and d_{Bi} are the diffusivity coefficients of interstitial; d_{Av} and d_{Bv} are the diffusivity coefficients of vacancies migrating via solute and matrix atoms, correspondingly; $g(\mathbf{r})$ is the source of solute atoms. The parameter ξ takes into account the non-random occupation of interstitials by A- and B-atoms; it is expressed in terms of the energy $H_{B\to A}$ gained by converting a B-interstitial (BB-dumbbell) into an A-interstitial (AB-dumbbell), $\xi = \exp(H_{B\to A}/k_B T)$ (k_B is the Boltzmann's constant and T is the temperature). In the case of dumbbell configurations, the conversion energy $H_{B\to A}$ equals the mixed-dumbbell binding energy.

Expressions for PD and solute fluxes can be obtained from a simple microscopic model of uncorrelated random walks of atoms via PD (for example, considering how atoms of different species exchange their positions between two adjacent atomic planes).

The limitation and applicability of Eqs. (1)–(5) are discussed in Ref. [14] in detail. Here we mention only that Eqs. (1)–(5) are valid for sufficiently concentrated alloys ($\min(C_A, C_B) > 10^{-3}$). For the sake of simplicity, the model ignores the correlation effects of diffusion and non-ideality of solid solution (the thermodynamic factor is set to unity). The expressions for the defect and solute fluxes with the correlation and thermodynamic factors are given in Refs. [16–18]. As distinct from other models [8,18,19] our model contains in explicit form the parameter ξ accounting for the possible deviation in the distribution of A- and B-interstitials from that prescribed by the formulae

$$C_i^{A,B} = C_i C_{A,B}. \tag{6}$$

The advantage of the model that we use is that it allows us to find analytical expressions with clear physical meaning. The set of Eqs. (1)–(5) is similar to the segregation model used by Wiedersich et al. [19] and Marwick [20]. At $\xi = 1$ our equations transform into equations of Ref. [19] provided that the thermodynamic factor in Ref. [19] is set to unity.

The source term $g(\mathbf{r})$ incorporated into the solute diffusion equation describes dissolution of precipitates due to cascades. Its origin should be discussed in some detail.

2.2. Cascade-induced dissolution of second phase precipitates

At sufficiently low temperatures, where thermally activated solid-state diffusion is frozen, direct displacement of atoms by the irradiating particle or in the cascade produced by it dominates the atomic migration. Being a random process, low temperature transport by collisional atomic displacements is directed towards destruction of any concentration inhomogeneity. Particularly pronounced effects are observed after cascade-producing neutron and ion irradiation. Mixing experiments are usually discussed in terms of two processes, ballistic mixing and thermal spike mixing [21,22]. Ballistic mixing involves two contributions, primary recoil mixing and cascade mixing. In the recoil mixing process, redistribution of atoms occurs through repeated single-collision events between the incident ion and target atoms. An initially displaced atom (primary recoil) may continue the knock-on-atom process producing a cascade of collision, replacement and displacement events in a spatially localized region. Such a mixing is referred to as cascade mixing. The lowest values of mixing efficiency $D_{\mathrm{mix}}/G = 0.1$ to 0.2 nm^2/dpa (where D_{mix} is the diffusion coefficient of tracers, and G is the displacement rate) measured in refractive metals are attributed to ballistic mixing [6]. According to molecular dynamics studies collective motion of atoms in a cascade ceases during times of several tens of picoseconds, a time period much longer than the ballistic phase [23,24]. At this stage the cascade may exhibit liquid-like properties, because temperatures in the cascade region derived from the estimated energy density may be much higher than the melting point of the material. Atomic mixing due to liquid-like diffusion during this thermal spike phase is assumed to be responsible for mixing efficiency in excess of the ballistic mixing. Molecular dynamics calculations on atomic mixing support the thermal spike concept [25]. In the following, we will use the term 'cascade mixing' to denote the atomic mixing in cascades due to all contributions.

In order to describe the disorder dissolution of the precipitate which is hit by cascades, the model of a cascade source [27,28] was used in Ref. [15]. Cascades are assumed to disorder the precipitate subsurface layer to a depth l_1 of about of the cascade size and eject the solute atoms into the matrix. Each cascade creates a concentration heterogeneity near the precipitate. Due to the thermal diffusion this heterogeneity relaxes recovering partially the precipitate. The relaxation lasts till another cascade hits the same region. Following the course of this process during a time interval exceeding the average time of successive cascade impacts in the same region of the precipitate, one can consider that the destruction of the surface layer leads to formation of a quasi-steady shell around the precipitate, which is locally enriched with the solute (Fig. 1). The thickness of this shell l is about of the cascade size or the average jump distance of atoms in a cascade. Generation of solute atoms near precipitates is described by the function $g(\mathbf{r})$ which is introduced as a source of solute atoms into the equation of solute diffusion, Eq. (2). Disorder produced by cascades within the precipitate is assumed to anneal very fast without any influence on precipitate evolution. Obviously, this model can be used only for precipitates larger than the cascade size.

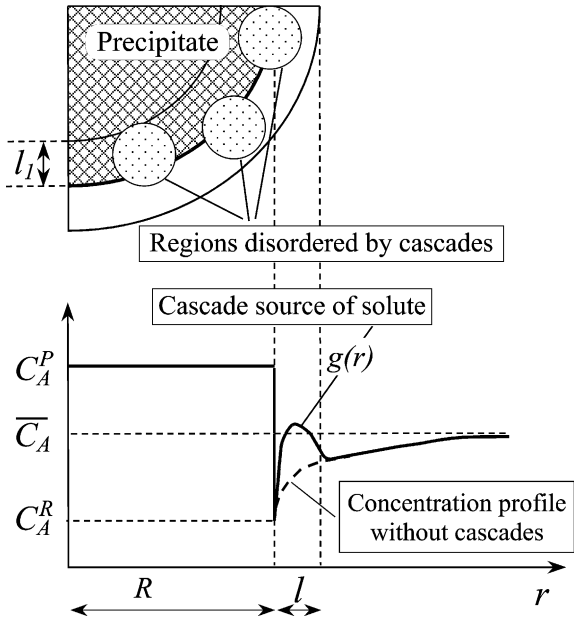

Fig. 1. Schematic view of cascade-induced dissolution of the spherical precipitate.

2.3. Criteria for stability of coherent and incoherent precipitates in binary alloy under irradiation

Considerable distinctions between growth rates of coherent and incoherent precipitates under irradiation have been revealed in Ref. [14]. Segregation dramatically affects the kinetics of evolution of incoherent precipitates under irradiation. The boundary of the incoherent precipitate contains a high density of defect sites, which offer trapping centers for PD. Persistent fluxes of vacancies and interstitials to the incoherent boundary results in segregation, i.e. in the preferential transport of one of the alloying elements toward the incoherent precipitate (the inverse Kirkendall effect [8]). Mutual

recombination of vacancies and interstitials at the precipitate boundary hinders backward diffusion of this element, by which affecting the growth and stability of the incoherent precipitate. The same is true for precipitates associated with PD sinks. Unlike the incoherent interface, the coherent interface, which is defined as one for which corresponding lattice planes and lines are continuous across the interface [26], being free of defect sites, is transparent to migrating PD and does not absorb them. For this reason radiation-induced segregation does not influence directly the stability of coherent precipitates. Atomic mixing in displacement cascades affects stability of precipitates of both types.

The conditions of precipitate stability can be formulated in terms of radiation-modified coherent and incoherent solubilities. For this purpose we find growth rates of coherent and incoherent precipitates. The diffusion equations are solved in the vicinity of an isolated precipitate embedded into the effective medium. All solute atoms are assumed to be either in the form of mobile monomers or combined with the constituent B to form large precipitates. Schematically, the growth rate of precipitates in the irradiated alloy is given by the expression

$$\frac{\mathrm{d}R_{\mathrm{coh,inc}}}{\mathrm{d}t} = \frac{D^{\mathrm{irr}}_{\mathrm{A\,coh,inc}}}{R(C^{\mathrm{P}}_{\mathrm{A}} - C^{\mathrm{R}}_{\mathrm{A}})}(\overline{C}_{\mathrm{A}} - C^{\mathrm{irr}}_{\mathrm{A\,coh,inc}}(R)), \tag{7}$$

which is similar to that for the case of unirradiated alloy [29]

$$\frac{\mathrm{d}R}{\mathrm{d}t} = \frac{D_{\mathrm{A}}}{R(C^{\mathrm{P}}_{\mathrm{A}} - C^{\mathrm{R}}_{\mathrm{A}})}(\overline{C}_{\mathrm{A}} - C^{\mathrm{R}}_{\mathrm{A}}), \tag{8}$$

where $C^{\mathrm{R}}_{\mathrm{A}}$ is the thermal equilibrium concentration of solute at the precipitate boundary; $\overline{C}_{\mathrm{A}}$ is the average concentration of solute in the matrix; $D^{\mathrm{irr}}_{\mathrm{A\,coh,inc}}$ is the coefficient of radiation-enhanced interdiffusion, which is different for coherent and incoherent precipitates [14]; D_{A} is the coefficient of thermal diffusion of solute; $C^{\mathrm{irr}}_{\mathrm{A\,coh,inc}}(R)$ is a function of $C^{\mathrm{R}}_{\mathrm{A}}$, diffusion parameters and irradiation conditions.

A comparison of Eqs. (7) and (8) shows that $C^{\mathrm{irr}}_{\mathrm{A\,coh,inc}}(R)$ plays the role of the equilibrium concentration of solute at the precipitate boundary. If the average solute concentration in the matrix equals $C^{\mathrm{irr}}_{\mathrm{A\,coh,inc}}(R)$ then the precipitate growth rate is zero. In other words, $C^{\mathrm{irr}}_{\mathrm{A\,coh,inc}}(R)$ determines the solute solubility under irradiation. By analogy with the thermal equilibrium concentration of solute $C^{\mathrm{e}}_{\mathrm{A}}$, we call the quantities

$$C^{\mathrm{irr}}_{\mathrm{A\,coh,inc}} = \lim_{R\to\infty} C^{\mathrm{irr}}_{\mathrm{A\,coh,inc}}(R), \tag{9}$$

the kinetically equilibrium solute concentrations or the radiation-modified solubilities.

The radiation-modified coherent $C^{\mathrm{irr}}_{\mathrm{A\,coh}}$ and incoherent $C^{\mathrm{irr}}_{\mathrm{A\,inc}}$ solubilities, being different, obey the equations (the derivation is given in Appendix A)

$$C^{\mathrm{irr}}_{\mathrm{A\,coh}} = C^{\mathrm{e}}_{\mathrm{A}} + \frac{D_{\mathrm{mix}}}{D^{\mathrm{irr}}_{\mathrm{A\,coh}}}(C^{\mathrm{P}}_{\mathrm{A}} - C^{\mathrm{e}}_{\mathrm{A}}), \tag{10}$$

$$\frac{C^{\mathrm{irr}}_{\mathrm{A\,inc}}}{1 - C^{\mathrm{irr}}_{\mathrm{A\,inc}}} = \frac{\widetilde{C}_{\mathrm{A}}}{1 - \widetilde{C}_{\mathrm{A}}} \times \left[1 + \left(\frac{\overline{C}_{\mathrm{v}}}{\widetilde{C}^{\mathrm{e}}_{\mathrm{v}}} - 1\right)\frac{1+\kappa}{1 + (\kappa - 1)C^{\mathrm{irr}}_{\mathrm{A\,inc}}}\right]^{(1-\kappa)/(1+\kappa)}, \tag{11}$$

where

$$\widetilde{C}_{\mathrm{A}} = C^{\mathrm{e}}_{\mathrm{A}} + \frac{D_{\mathrm{mix}}}{D^{\mathrm{irr}}_{\mathrm{A\,inc}}}(C^{\mathrm{P}}_{\mathrm{A}} - C^{\mathrm{e}}_{\mathrm{A}}), \tag{12}$$

$$\widetilde{C}^{\mathrm{e}}_{\mathrm{v}} = C^{\mathrm{e}}_{\mathrm{v}} + \frac{d_{\mathrm{Av}} - d_{\mathrm{Bv}}}{d_{\mathrm{Av}}d_{\mathrm{Bv}}}D_{\mathrm{mix}}(C^{\mathrm{P}}_{\mathrm{A}} - C^{\mathrm{e}}_{\mathrm{A}}) \tag{13}$$

and the coherent and incoherent coefficients of interdiffusion are determined by

$$D^{\mathrm{irr}}_{\mathrm{A\,coh}} = \frac{d_{\mathrm{Av}}d_{\mathrm{Bv}}\overline{C}_{\mathrm{v}}}{\overline{D}_{\mathrm{v}}} + \frac{\lambda\overline{D}_{\mathrm{i}}\overline{C}_{\mathrm{i}}}{(\overline{C}_{\mathrm{B}} + \lambda\overline{C}_{\mathrm{A}})(C^{\mathrm{R}}_{\mathrm{B}} + \lambda C^{\mathrm{R}}_{\mathrm{A}})}, \tag{14}$$

$$D^{\mathrm{irr}}_{\mathrm{A\,inc}} = \frac{d_{\mathrm{Av}}d_{\mathrm{Bv}}C^{\mathrm{e}}_{\mathrm{v}}}{d_{\mathrm{Bv}}C^{\mathrm{e}}_{\mathrm{B}} + d_{\mathrm{Av}}C^{\mathrm{e}}_{\mathrm{A}}}. \tag{15}$$

Here and henceforth the bar denotes the average values, the superscript R refers to quantities at the precipitate-matrix interface. $D_{\mathrm{mix}} = 0.5 l_1 l \gamma K \equiv d_{\mathrm{mix}}K$ has the meaning of the diffusion coefficient due to cascade mixing, (γ is the number of replacements per the Frenkel pair survived the cascade relaxation, i.e. the efficiency of atomic mixing), and $\kappa = \xi d_{\mathrm{Ai}}d_{\mathrm{Bv}}/d_{\mathrm{Bi}}d_{\mathrm{Av}}$ is the parameter indicating the direction of solute segregation

- at $\kappa > 1$ solute is enriched at sinks,
- at $\kappa < 1$ solute segregates away from sinks [14].

The second multiplier in Eq. (11) arises due to radiation-induced segregation, while the first one describes an increase of solubility due cascade mixing (compare Eq. (12) to Eq. (10)).

Eqs. (10) and (11) for $C^{\mathrm{irr}}_{\mathrm{A\,coh,inc}}$ are not closed because the average concentrations of PD enter these equations. In its turn, the average PD concentrations depend on radiation-modified solubilities. Let us express the concentrations $\overline{C}_{\mathrm{i,v}}$ in terms of the displacement rate, the parameters of alloy microstructure and the average solute concentration. For this purpose we will construct the balance equations for concentrations of PD.

2.4. The effective medium approach for binary alloy under irradiation

Along with precipitates of second phases real alloys contain structural defects of other types: voids, dislocations, grain boundaries, etc., which absorb radiation-induced PD. For pure metal the problem of determinations of PD fluxes to sinks is usually considered within the framework of the approach of an effective lossy medium [30,31]. The essence of this approach consists in a reduction of a many-body problem to a one-body problem, i.e. instead of solving the microscopic continuity equations for concentrations of PD with boundary conditions at all sinks one solves a diffusion problem in a neighborhood of an isolated sink, all remaining sinks being substituted by a homogeneous effective lossy medium. In this section, following the previous papers [14,32] we will outline briefly the model of the effective lossy medium for a binary substitutional alloy.

Consider Eqs. (1)–(5) at the quasi-steady-stage ($\partial C_{i,v}/\partial t \equiv \dot{C}_{i,v} = 0$). Averaging over all possible sink configurations and the volume containing a large number of sinks yields

$$K - \alpha_R \overline{D}_i \overline{C}_i \overline{C}_v - \sum_j N_j J_n^j = 0, \quad n = i, v, \tag{16}$$

where N_j is the density of sinks of j-type, namely, voids (N_V), incoherent precipitates (N_P) and edge dislocations ($N_d = \rho$). J_n^j is the PD flux to the sink of j-type.

PD fluxes to voids and dislocations can be found from the diffusion problem similar to that of incoherent precipitate growth. If $\overline{C}_A > C_{A\,inc}^{irr}$, then in the course of time PD sinks are covered with second phase layers. In this case

$$J_i^j = Z_j \overline{D}_i \overline{C}_i,$$

$$J_v^j = Z_j D_v^{eff} \left[\overline{C}_v - C_v^e - \frac{d_{Av} - d_{Bv}}{d_{Av} d_{Bv}} \times \left(\frac{\dot{\Omega}_j}{Z_j} + D_{mix}(C_A^P - C_A^e) \right) \right], \tag{17}$$

where

$$D_v^{eff} = d_{Bv} \frac{1 + (\lambda - 1)\overline{C}_A}{1 + (\kappa - 1)\overline{C}_A}, \tag{18}$$

$$Z_{V,P} = 4\pi R_{V,P}, \qquad Z_d = 2\pi \left(\ln \frac{R_{inf}}{R_d} \right)^{-1},$$

$$\dot{\Omega}_{V,P} \equiv (C_A^P - C_A^e)\dot{V}_{V,P}, \quad \dot{\Omega}_d \equiv (C_A^P - C_A^e)\dot{S},$$

and $R_{V,P}$ are the void and precipitate radii, correspondingly, R_d is the capture radius of PD by a dislocation, R_{inf} is about of the average distance between sinks, $\dot{V}_{V,P}$ is the growth rate of the volume of the second phase layer around the void or the volume of the separate precipitate, respectively; $\dot{S}$ is the growth rate of the cross-section of a precipitate attached to a dislocation.

Since we are looking for the solute concentrations, which determine the precipitate stability thresholds, in Eq. (17) we should set precipitate growth rates to zero, $\dot{\Omega}_j = 0$, at $C_{A\,coh,inc}^{irr}$. In this case the balance equations are reduced to the form

$$K - \alpha_R \overline{D}_i \overline{C}_i \overline{C}_v - k^2 \overline{D}_i \overline{C}_i = 0, \tag{19}$$

$$K - \alpha_R \overline{D}_i \overline{C}_i \overline{C}_v - k^2 D_v^{eff} (\overline{C}_v - \widetilde{C}_v^e) = 0, \tag{20}$$

where k^2 is the total sink strength determined by the relations

$$k^2 = \begin{cases} \overline{Z}_V N_V + Z_d \rho + \overline{Z}_P N_P & \text{at } \overline{C}_A \geqslant C_{A\,inc}^{irr}, \\ \overline{Z}_V N_V + Z_d \rho & \text{at } \overline{C}_A < C_{A\,inc}^{irr}, \end{cases} \tag{21}$$

$$\widetilde{C}_v^e = \begin{cases} C_v^e + \frac{d_{Av} - d_{Bv}}{d_{Av} d_{Bv}} D_{mix}(C_A^P - C_A^e) & \text{at } \overline{C}_A \geqslant C_{A\,inc}^{irr}, \\ C_v^e & \text{at } \overline{C}_A < C_{A\,inc}^{irr}. \end{cases} \tag{22}$$

The solution of Eqs. (19) and (20) yields the average PD concentrations

$$\overline{D}_i \overline{C}_i = D_v^{eff} (\overline{C}_v - \widetilde{C}_v^e), \tag{23}$$

$$\overline{C}_v - \widetilde{C}_v^e = 0.5 \left(\widetilde{C}_v^e + \frac{k^2}{\alpha_R} \right) \times \left\{ \sqrt{1 + \frac{4K}{\alpha_R D_v^{eff}} \left(\widetilde{C}_v^e + \frac{k^2}{\alpha_R} \right)^{-2}} - 1 \right\}. \tag{24}$$

It should be noted that the rate Eqs. (19) and (20) are similar to the equations of the effective lossy medium approach for pure metals. The difference is that in the alloy under irradiation the effective diffusion coefficient of vacancies (Eq. (18)) depends on kinetic coefficients of interstitials and on average solute concentration [14].

Eqs. (10) and (11) together with Eqs. (23) and (24) for the average concentrations of PD form the complete set of equations that determines the radiation-modified solubilities.

3. Application of the model to Zr–Nb alloys

Zr–Nb alloys are normally fabricated with a dual α-Zr + β-Zr phase structure. According to the equilibrium phase diagram, the β-Zr phase (the bcc lattice, about 20 at.% Nb) is thermally unstable under operating temperatures of thermal reactors (for example,

Zr–2.5Nb pressure tubes in CANDU reactors contain a hot primary coolant at about 520 to 570 K). The hcp α-phase is also metastable, having a composition greater than the equilibrium value, i.e. supersaturated with Nb.

The metastable β-Zr phase undergoes a sequence of complex transformation. Under neutron irradiation ($E > 1$ MeV, fluences up to 25×10^{25} n/m^2) at temperatures between 520 and 570 K the β-Zr phase structure is modified, but it appears that irradiation suppresses any further thermal decomposition [33,34]. However, in Ref. [35] the experimental results on decomposition of the β-Zr phase in the Zr–2.5Nb alloy under 3.6 MeV proton irradiation are presented. After irradiation with the dose rate 9.2×10^{-7} dpa/s at 770 K (18 h) and 720 K (264.5 h) to a dose of about 1 dpa the β-Zr phase decomposed into an array of individual platelet or needle-like precipitates of β-Nb phase with the niobium content up to 90% [35]. Probably the discrepancy between two observations is explained by different displacement rates and irradiation temperatures.

In this paper we do not consider evolution of the β-Zr phase under irradiation. We are interested in precipitation and stability of β-Nb phase in the α-Zr matrix. According to numerous observations irradiation clearly has an effect on the production of β-Nb precipitates in the α-phase. The radiation-enhanced β-Nb precipitation in the form of needles, platelets or sword-shaped precipitates has been observed under electron [36] proton [35] and neutron [33,34,37–40] irradiation. Experimental evidences are:

- In irradiated samples the average size of β-Nb precipitates is generally very small, 5–40 nm in length. Though, β-Nb precipitates of larger sizes, 30–200 nm, were observed in a 40% cold-worked Zr–2.5Nb (E125) pressure tube irradiated in RBMK-1000 at 577 K to high neutron fluences (up to 10^{26} n/m^2, $E > 1$ MeV) [40].
- The density of precipitates is high and generally they are distributed uniformly within the α-Zr phase. (However, there is an indirect evidence that under neutron irradiation at temperatures as high as 770 K β-Nb precipitates can occur preferentially at dislocations [37].)
- Nucleation and growth of β-Nb precipitates are difficult without irradiation since no precipitation occurred during aging for 1500 h at temperatures as high as 770 K [37]. In out of flux sections of pressure tubes there were also no observations of Nb precipitation [33,34] indicating that radiation-enhanced diffusion kinetics plays an important role in the precipitation process.
- Formed precipitates are stable. The β-Nb did not dissolve during heating at 770 K for 1000 h, but that formed during neutron irradiation at 570 and 670 K grew larger [37]. A similar behavior was observed after electron irradiation [36].
- There are many examples showing a zone denuded of β-Nb precipitates adjacent to β-phase or grain boundaries both under electron [36] and neutron irradiation [34,37].
- The improved corrosion resistance in Zr–2.5Nb pressure tubes due to irradiation correlates with Nb precipitation in the α-phase of Zr–2.5Nb (see for example, Ref. [34] and papers cited there).

We have not found in the literature observations of large incoherent globular Nb precipitates or precipitates at grain boundaries in the α-Zr phase irradiated under reactor conditions, i.e. at temperatures below 600 K. In our opinion, this indicates that these precipitates are unstable under irradiation and therefore cannot grow. At the same time, stability of small platelet or needle-like precipitates under irradiation can be understood if we consider them coherent with the α-Zr matrix. In reality, β-Nb particles cannot be fully coherent with the α-matrix because of different crystal lattices. Spherical or globular precipitates have the smallest surface area at a given volume; but, because of lattice misfit, they are incoherent with the matrix. It is known that the specific surface energy of the incoherent interface is larger than that of the coherent interface. Hence, the incoherent precipitate would have a large interface energy. That is the reason why the β-Nb phase precipitates in the form of needles, platelets or sword-shaped particles. Most of the interface of such a precipitate is coherent with the matrix, while the lattice misfit is accommodated at the incoherent fraction of the interface, which is small as compared to the coherent one. For example, it is likely that the β-Nb platelet is coherent with the matrix in the plane of plate, while its edge is incoherent (similarly to the η-phase platelets in an austenitic stainless steel [41]). The coherent fraction of the precipitate interface can dominate in the segregation behavior of the precipitate, so that on the average the β-Nb platelet can be considered coherent (or semi-coherent) with the matrix.

There are two possible mechanisms which can be responsible for the absence of large incoherent precipitates: (i) the radiation-induced segregation and (ii) the cascade-induced dissolution or sputtering. In irradiated alloys segregation effects arise due to the coupling between fluxes of alloying elements and PD fluxes, as well as due to differences in the diffusion rates of solute and solvent atoms when migrating via a vacancy or interstitial mechanisms [1,19]. The point is that the radiation-sustained defect fluxes toward a sink (incoherent precipitate or grain boundary) lead to the preferential transport of one of the alloying elements to that sink, but the backward diffusion of this element is hindered because of mutual recombination of vacancies and interstitials at the sink surface. For this reason compositional gradients form around sinks. If the Nb segregates away from PD sinks this results in formation of Nb depleted zones adjacent to sinks. This means that if we put an incoherent β-Nb precipitate into the α-Zr matrix supersaturated with Nb, a zone undersaturated with Nb

would form around this precipitate under irradiation, which results in precipitate dissolution. Consequently, such precipitates are unstable and cannot grow under irradiation. The same is true for precipitates associated with grain boundaries or situated in the vicinity of gain boundaries – they cannot form in a locally undersaturated solid solution of Nb in the α-phase. Another process that destabilizes incoherent precipitates is the cascade mixing. Displacement cascades dissolve coherent and incoherent precipitates with the equal efficiency determined by D_{mix} (see Eqs. (10)–(12)). However, the rates of precipitate recovery, which are proportional to interdiffusion coefficient, differ. The reason is that the interdiffusion coefficient depends on PD concentrations in the vicinity of precipitate. PD concentrations differ near the boundaries of coherent and incoherent precipitates [14]. PD concentrations near coherent precipitates equal the average concentrations. Near incoherent precipitates these concentrations equal the thermal equilibrium values. As a result, the interdiffusion coefficient near coherent precipitates exceeds considerably the interdiffusion coefficient near incoherent precipitates ($D^{\mathrm{irr}}_{\mathrm{A\,coh}}/D^{\mathrm{irr}}_{\mathrm{A\,inc}} \propto \overline{C}_{\mathrm{v}}/C^{\mathrm{e}}_{\mathrm{v}} \gg 1$, see (Eqs. (14) and (15)). Obviously, there exists a critical temperature below which the cascade-induced dissolution dominates the diffusion recovery of precipitates. For incoherent precipitates this temperature is higher than that for coherent precipitates. The calculations presented in Section 3.2 confirm this conclusion.

To find radiation-modified coherent and incoherent solubilities and to construct the radiation-modified phase diagram of Zr–Nb alloy the set of Eqs. (10), (11), (23) and (24) was solved numerically. Diffusivity coefficients were taken in the form

$$d_{\mathrm{Nn}} = d_{\mathrm{n0}} \exp(-E^{\mathrm{m}}_{\mathrm{Nn}}/k_{\mathrm{B}}T), \tag{25}$$

where N = Zr, Nb; n = i, v; $E^{\mathrm{m}}_{\mathrm{Nn}}$ is the migration energy of the corresponding defect. The main difficulty was the choice of diffusion parameters. We did not find in the literature either the diffusivity parameters of vacancies ($d_{\mathrm{Nb\,v}}$ and $d_{\mathrm{Zr\,v}}$) and interstitials ($d_{\mathrm{Nb\,i}}$ and $d_{\mathrm{Zr\,i}}$) or reliable measurement of segregation profiles, which can be used for evaluation of these parameters. Another point is that small amounts of impurities such as Fe strongly influence both the value and the anisotropy ratio of vacancy diffusion in Zr alloys [42]. In the following to estimate the location of phase boundaries in irradiated Zr–Nb alloys, we assume that the alloy is isotropic and use the self-diffusion data for α-Zr single crystals [43]. The direction of segregation depends on ratios $\xi d_{\mathrm{Ai}}/d_{\mathrm{Bi}} = \xi d_{\mathrm{Nb\,i}}/d_{\mathrm{Zr\,i}}$ and $d_{\mathrm{Av}}/d_{\mathrm{Bv}} = d_{\mathrm{Nb\,v}}/d_{\mathrm{Zr\,v}}$, i.e. on the relations between activation energies

$$\Delta E_{\mathrm{i}} = E^{\mathrm{m}}_{\mathrm{Zr\,i}} - E^{\mathrm{m}}_{\mathrm{Nb\,i}} + H_{\mathrm{Zr\to Nb}},$$
$$\Delta E_{\mathrm{v}} = E^{\mathrm{m}}_{\mathrm{Zr\,v}} - E^{\mathrm{m}}_{\mathrm{Nb\,v}}.$$

The β-Nb precipitates are assumed to consist of pure Nb. This is reasonable because of uncertainty of other physical parameters. The Nb solubility in Zr [46] we approximate by the analytical expression. The alloy parameters are presented in Table 1.

3.1. Cascade-free irradiation

The electron irradiation can be considered a pure PD generator, with no cascades. Mixing efficiency of electron irradiation is much smaller than that of cascade-producing irradiation; therefore, as a zero approximation, we can set $d_{\mathrm{mix}} = 0$. According to Eq. (10) irradiation does not modify the coherent solubility, $C^{\mathrm{irr}}_{\mathrm{A\,coh}} = C^{\mathrm{e}}_{\mathrm{A}}$, whereas the incoherent solubility changes due to segregation effects (Eqs. (11)–(13)). Fig. 2 shows the radiation-modified phase diagram calculated for two cases:

(a) Nb segregates away from PD sinks, $\kappa = \xi d_{\mathrm{Ai}} d_{\mathrm{Bv}}/d_{\mathrm{Bi}} d_{\mathrm{Av}} < 1$, and
(b) Nb segregates to PD sinks, $\kappa > 1$.

In both cases, the stability field of incoherent precipitates is situated to the left of solid curves.

Table 1
Material parameters of Zr–Nb alloy used in calculations of radiation-modified solubilities

Parameter	Value	Reference
Displacement rate, K (dpa/s)	10^{-7}	
Cascade mixing efficiency, d_{mix} (nm^2)	4.2; 0.01	
Nb solubility in Zr, $C^{\mathrm{e}}_{\mathrm{A}} \equiv C^{\mathrm{e}}_{\mathrm{Nb}}$ (atomic fraction)	$0.014\exp(-0.06\ \mathrm{eV}/k_{\mathrm{B}}T)$	[46]
Recombination rate constant, α_{R} (m^{-2})	3×10^{20}	
Sinks strength, k^2 (m^{-2})	5×10^{14}; 5×10^{15}	
Zr self-diffusion coefficient, $D_{\mathrm{Zr\,v}} = D_{\mathrm{Zr\,0}} \exp(-(E^{\mathrm{f}}_{\mathrm{Zr\,v}} + E^{\mathrm{m}}_{\mathrm{Zr\,v}})/k_{\mathrm{B}}T)$ (m^2/s)	$9 \times 10^{-5}\exp(-3.17\ \mathrm{eV}/k_{\mathrm{B}}T)$	[43]
Equilibrium vacancy concentration in Zr, $C^{\mathrm{e}}_{\mathrm{v}} = C_{\mathrm{v0}} \exp(-E^{\mathrm{r}}_{\mathrm{Zr\,v}}/k_{\mathrm{B}}T)$ (atomic fraction)	$0.54\exp(-1.8\ \mathrm{eV}/k_{\mathrm{B}}T)$	[45]
Thermal diffusion coefficient of vacancies in Zr, $d_{\mathrm{Zr\,v}} = d_{\mathrm{v0}} \exp(-E^{\mathrm{m}}_{\mathrm{Zr\,v}}/k_{\mathrm{B}}T)$ (m^2/s)	$1.67 \times 10^{-4}\exp(-1.37\ \mathrm{eV}/k_{\mathrm{B}}T)$	[43,45]

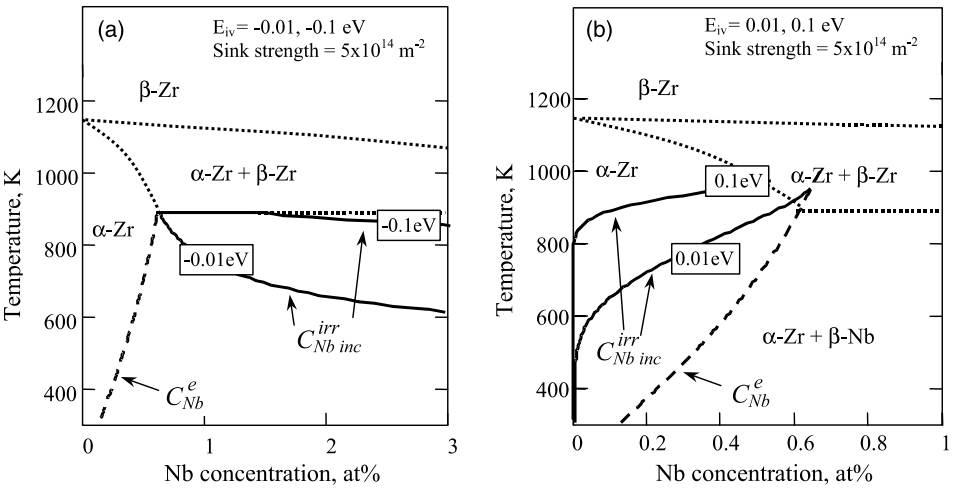

Fig. 2. Radiation-modified phase under cascade-free irradiation. The equilibrium phase diagram [50] is shown by dotted lines as a reference. Solid curves are incoherent solubilities. The dashed curve is the coherent solubility that coincides with the thermal solubility. The stability field of incoherent precipitates is located to the left of solid curves. Labels at the curves indicate numerical values of the parameter $E_{iv} = \Delta E_i - \Delta E_v$. (a) Corresponds to the case of Nb segregating away from PD sinks ($\kappa < 1$); (b) corresponds to the case of Nb segregating to PD sinks and incoherent precipitates ($\kappa > 1$).

The situation depicted in Fig. 2(b) does not agree with experimental observations. If the Nb segregates to sinks, one would observe the formation of β-Nb precipitates at grain boundaries rather than precipitate depleted zones [36]. Therefore, it is likely that the Nb segregates away from the PD sinks (Fig. 2(a)). This means that under irradiation near PD sinks the solid solution is undersaturated with Nb, hence, no β-Nb precipitates can nucleate. It is interesting to note that even very small difference in diffusivity parameters, $E_{iv} = \Delta E_i - \Delta E_v \sim -0.01$ eV, results in appearance of a well-defined low temperature threshold for stability of incoherent precipitates. According to Fig. 2(a), at $E_{iv} \sim -0.01$ eV and $T < 600$ K no incoherent precipitates can exist under irradiation with $K = 10^{-7}$ dpa/s. At $E_{iv} \sim -0.1$ eV the low temperature threshold is close to the monotectoid temperature. At numerical values of parameters used in this paper and for $|E_{iv}| < 1$ eV the radiation-modified incoherent solubility is well described by the simple formula

$$C^{irr}_{A\,inc} = C^{e}_{A}\left[1 + \left(\frac{\overline{C}_v}{C^{e}_v} - 1\right)(1+\kappa)\right]^{(1-\kappa)/(1+\kappa)}, \qquad (26)$$

where the vacancy supersaturation is given by the expression similar to that for pure metals

$$\frac{\overline{C}_v}{C^{e}_v} - 1 = 0.5\left(1 + \frac{k^2}{C^{e}_v \alpha_R}\right) \times \left\{\sqrt{1 + \frac{4K}{\alpha_R d_{Zr\,v}\left(C^{e}_v + \frac{k^2}{\alpha_R}\right)^{-2}}} - 1\right\}. \qquad (27)$$

If one accepts that the α-Zr phase is in a supersaturated state prior to irradiation, then the decomposition of the α-Zr phase is understandable based on the unmodified phase diagram. However, the rates of decomposition under irradiation and during thermal annealing may differ considerably. As an example, we will cite the results on electron irradiation of Zr–2.5Nb alloy [36]. The irradiation with 10 MeV electrons at 710 K to about 1 dpa enhances the precipitation of β-Nb precipitates in the α-Zr phase of annealed Zr–2.5Nb alloy. The microstructure of the irradiated material contained needle-like precipitates in the grain interior. Denuded zones were observed at the grain boundaries with a thickness of about 100 nm. The precipitates, with a 1 to 2 nm range in width and a maximum length of 70 nm, were embedded completely in the α-Zr grains. An analysis revealed that the precipitates were β-Nb particles, while the α-Zr grain interior did not contain a significant amount of Nb. A sample of the same unirradiated Zr–2.5Nb material was annealed at 720 K for 370 h, the same time period as the electron irradiation; TEM examination shown that the precipitates seen after electron irradiation were not formed by thermal aging. At the same time a post-irradiation anneal at 720 K for 500 h caused no significant changes in the population of β-Nb precipitates in irradiated samples [36]. These results demonstrate that (i) the observed β-Nb precipitation is radiation-enhanced and (ii) the decomposition kinetics without irradiation is slow.

An estimate based on the equation of diffusion-limited growth of a spherical precipitate (a simplified

version of Eq. (7)) gives the idea about time scales involved in decomposition of the Zr–Nb solid solution.

$$\frac{dR}{dt} \leqslant \frac{D_{Nb}}{R}\overline{C}_{Nb}, \tag{28}$$

where $\overline{C}_{Nb}$ is the Nb concentration in the solid solution and D_{Nb} is the Nb diffusion coefficient which in segregation-free case is given by

$$D_{Nb} = \begin{cases} d_{Zr\,v}C_v^e & \text{thermal aging,} \\ d_{Zr\,v}(2\overline{C}_v - C_v^e) & \text{under irradiation.} \end{cases} \tag{29}$$

It follows from Eq. (28) that the time necessary for the precipitate to grow to a radius R is given by

$$\tau \geqslant \frac{R^2}{2D_{Nb}\overline{C}_{Nb}}. \tag{30}$$

If we assume that β-Nb precipitates nucleate very fast then Eq. (30) provides an estimate for the minimum time required for solid solution decomposition. As a precipitate radius one can take a value when precipitates become visible in a transmission electron microscope, for example, $R = 2$ nm. According to Eqs. (29) and (30), irradiation decreases the lifetime of a metastable supersaturated state by a factor of $\overline{C}_v/C_v^e$. Fig. 3 shows the temperature dependence of the decomposition time plotted for thermal aging and irradiation. It is seen that

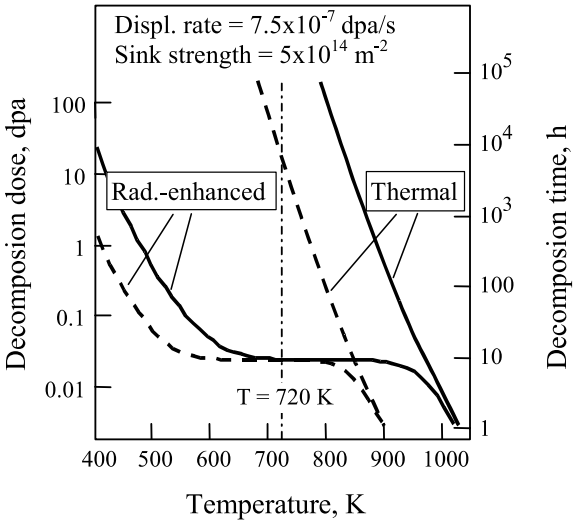

Fig. 3. Temperature dependence of the decomposition time given by Eq. (30) for thermal aging and irradiation with the displacement rate corresponding to the electron irradiation used in Ref. [36]. Solid lines were calculated with the vacancy formation and migration energies indicated in Table 1. For dashed lines corresponding energies were reduced by 0.2 eV. The dash-dotted line shows the temperature of thermal aging carried out in [36]. The Nb concentration in solid solution $C_{Nb} = 0.02$ and the precipitate radius $R = 2$ nm.

even if we reduce the vacancy formation and migration energies (taking into account the enhancement of Zr self-diffusion in the Zr–Nb alloys [43,44] and influence of impurities on Zr self-diffusion), without irradiation the decomposition is still slow at temperatures below 800 K.

3.2. Cascade-producing irradiation

Atomic mixing in displacement cascades prevents precipitates from growth and tends to increase both coherent and incoherent solubilities. Fig. 4 shows the radiation-modified phase diagram calculated at a dose rate of $K = 10^{-7}$ dpa/s (typical for thermal reactors), assuming that there is no radiation-induced segregation ($\Delta E_i = \Delta E_v = 0$). It is seen that the stability threshold for incoherent β-Nb precipitates is located in the phase diagram at temperatures close to the temperature of the thermodynamic stability of the β-Nb phase. This means that incoherent β-Nb precipitates are unstable under reactor conditions. According to Eqs. (10)–(15) and (24), in the segregation-free case the location of low-temperature stability thresholds for incoherent and coherent precipitates can be estimated by

$$T_{inc} = \frac{E_{Zr\,v}^f + E_{Zr\,v}^m}{k_B}\left(\ln\frac{d_{v0}C_{v0}Q}{d_{mix}K}\right)^{-1}, \tag{31}$$

$$T_{coh} = \frac{E_{Zr\,v}^m}{k_B}\left(\ln\frac{4d_{v0}Q^2}{d_{mix}^2\alpha_R K}\right)^{-1}, \tag{32}$$

where Q is the Nb content in the alloy (in atomic fractions).

As can be expected, with mixing efficiency decreasing both low temperature thresholds decrease (Fig. 5). It is important that even at a very low mixing efficiency the threshold for stability of incoherent precipitates is located at rather high temperatures. The reason is that T_{inc} depends on d_{mix} logarithmically, as well as the Zr self-diffusion energy is high.

Note that the cascade-producing irradiation at temperatures below the threshold temperature for coherent precipitate stability inhibits the growth of large precipitates in a thermodynamically unstable solid solution and keeps the precipitate sizes below a value of about of the cascade size, i.e. a steady-state size distribution of precipitates forms. Because of existence of two thresholds for precipitate stability, T_{coh} and T_{inc}, the steady-state size distribution of precipitates can be produced in Zr–Nb alloy under irradiation even at temperatures higher than the low temperature coherent threshold. The interval of operating temperatures of pressure tubes is situated between these two thresholds (Figs. 4 and 5). Under neutron irradiation at these temperatures the coherent β-Nb precipitates are stable in Zr with a few percents of Nb; they nucleate, grow and coarsen with radiation-enhanced rate. As the precipitates grow, they lose the coherency because of accumulation of excess

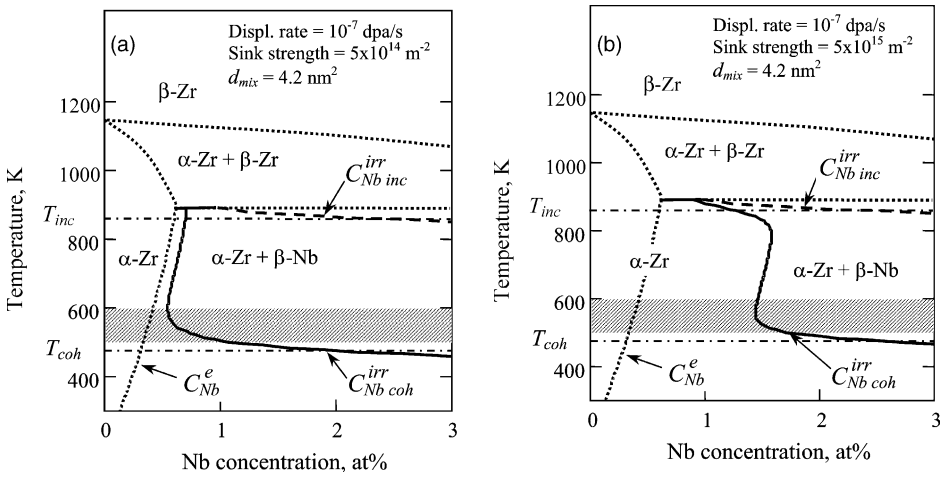

Fig. 4. Radiation-modified phase diagram of Zr–Nb alloy calculated for cascade-producing irradiation without segregation effects ($\Delta E_i = \Delta E_v = 0$) at different sink strengths. For comparison the equilibrium phase diagram [50] is shown by dotted lines. Low-temperature thresholds T_{inc} and T_{coh} correspond to volume fraction of Nb $Q = 0.015$. Shading shows a typical interval of pressure tube operating temperatures.

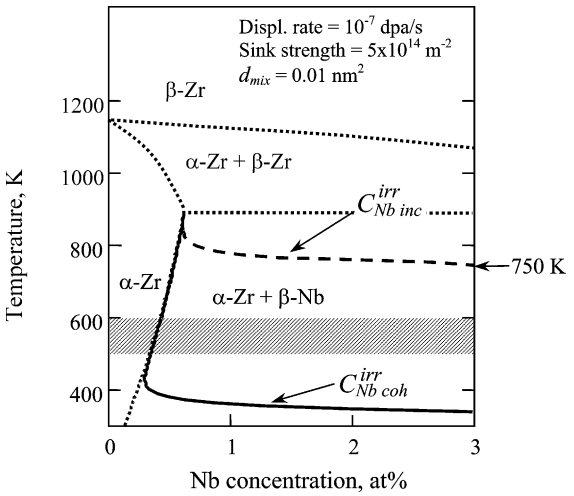

Fig. 5. Radiation-modified phase diagram of Zr–Nb alloy calculated for cascade-producing irradiation without segregation effects ($\Delta E_i = \Delta E_v = 0$) at sink strengths 5×10^{14} m^2. Shading shows a typical interval of pressure tube operating temperatures. Note that the mixing efficiency was reduced by factor of 400 as compared to that in Fig. 4.

energy connected with the misfit between the α-matrix and precipitates. [1] However, globular incoherent precipitates are unstable because their field of stability is located at higher temperatures (Figs. 4 and 5). The incoherent precipitates dissolve completely or partially (if the coherency is restored) resulting in solute enrichment in the matrix and renucleation of new coherent precipitates. Due to competition between these processes a steady-state size distribution forms.

The shape of the radiation-modified coherent solvus depends on sink strength. In the temperature range of 550–800 K the radiation-modified coherent solvus is parallel to the thermal one (Fig. 4(b)). At these temperatures PD are lost predominantly to sinks. For this reason the coefficient of radiation-enhanced interdiffusion, $D^{irr}_{A\,coh}$, is almost independent of temperature (compare with Fig. 3), hence, according to Eq. (10), the radiation-modified coherent solubility follows the temperature dependence of the thermal solvus. The distance along the concentration axis between the radiation-modified coherent solubility and the thermal one is given by

$$\delta C_A = 0.5 d_{mix} k^2 (C^P_A - C^e_A). \quad (33)$$

Fig. 6(a) and (b) represents the radiation-modified diagrams when Nb is assumed to segregate to sinks via the interstitial mechanism ($\Delta E_i > 0$). It is seen that incoherent precipitates can exist in the region of undersaturated solid solution. However, despite very strong segregation of Nb to sinks, the low temperature incoherent threshold is located at rather high temperatures even at very low mixing efficiency (Fig. 6(b)). Fig. 6(c) and (d) was constructed with the assumption that Nb segregates away from sinks. Comparison of Figs. 5 and 6(d) show that segregation effects shifts the incoherent solubility curve to higher temperatures.

Analytical estimations based on the model and their comparison with numerical calculations show that at any values of $\Delta E_{i,v}$ and at fixed diffusion parameters of

[1] It is known that irradiation may accelerate the coherency loss [47–49].

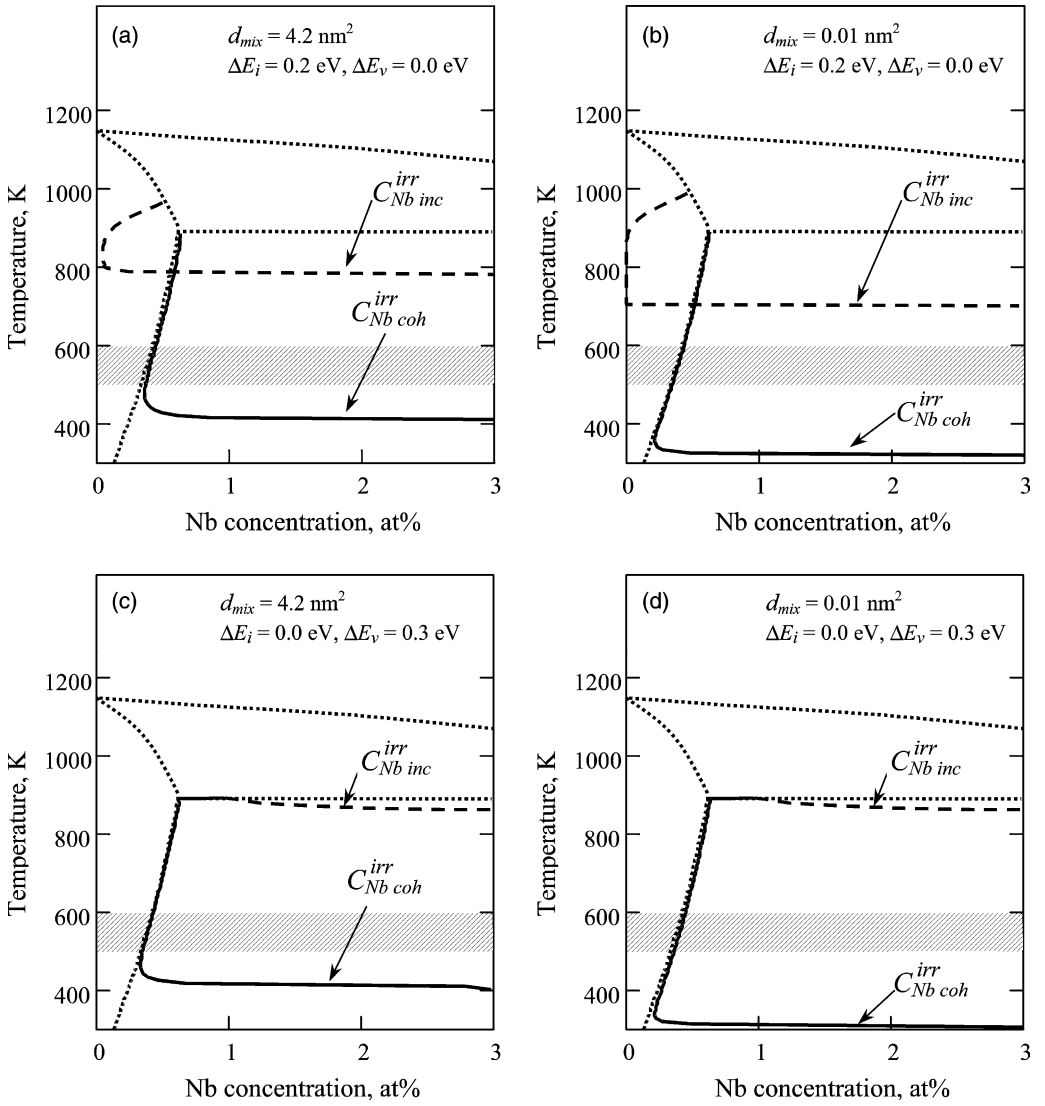

Fig. 6. Radiation-modified phase diagram of Zr–Nb alloy showing the combined influence of radiation-induced segregation and cascade mixing on the coherent and incoherent solubilities. Figures (a) and (b) correspond to the case of Nb segregating to PD sinks ($\kappa > 1$); figures (c) and (d) correspond to the case of Nb segregating away from PD sinks and incoherent precipitates ($\kappa < 1$). Dose rate 10^{-7} dpa/s, sink strength 5×10^{14} m^{-2}. For comparison the equilibrium phase diagram [50] is shown by dotted lines. Shading shows a typical interval of pressure tube operating temperatures.

Zr the low-temperature thresholds can not be located below

$$T^{\min}_{\text{inc}} = \frac{E^{\text{f}}_{\text{Zr v}} + E^{\text{m}}_{\text{Zr v}}}{k_{\text{B}}} \left(\ln \frac{d_{\text{v0}} C_{\text{v0}}}{d_{\text{mix}} K} \right)^{-1}, \tag{34}$$

$$T^{\min}_{\text{coh}} = \frac{E^{\text{m}}_{\text{Zr v}}}{k_{\text{B}}} \left(\ln \frac{4 d_{\text{v0}}}{d^2_{\text{mix}} \alpha_{\text{R}} K} \right)^{-1}. \tag{35}$$

The dependence of low-temperature thresholds on displacement rate is depicted in Fig. 7. These relations may be useful in practical assessment of phase stability.

4. Discussion

We have formulated the model for phase stability loss under irradiation. The radiation-modified phase diagram of Zr–Nb alloy was constructed. The model gives an insight into the system behavior at high doses and reveals the microstructural and material parameters that control the development of phase composition. Surely, in the present state the model cannot be directly used for prediction of evolution of complex commercial alloys. However, it can be used as a basis for more detailed description.

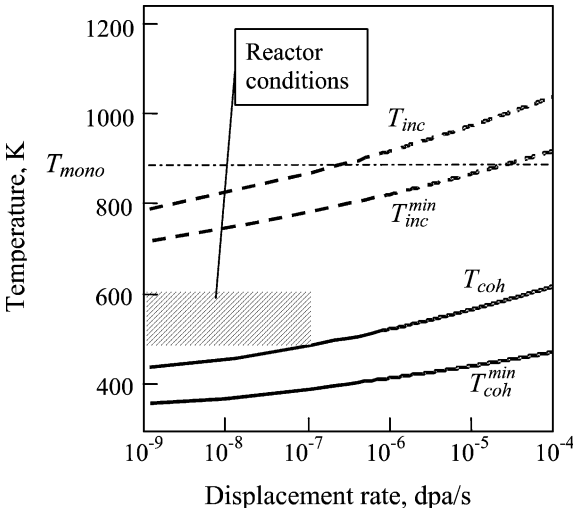

Fig. 7. Dependence of low-temperature thresholds for precipitate stability on displacement rate. T_{mono} is the monotectoid temperature above which β-Nb phase is thermodynamically unstable. The thresholds were calculated with Eqs. (31), (32), (34) and (35) at volume fraction of Nb $Q = 0.015$ and $d_{\mathrm{mix}} = 4.2$ nm^2. Shading shows in-reactor operating conditions for pressure tubes.

The cascade-free electron irradiation modifies the incoherent solubility because of radiation-induced segregation of alloying elements at the incoherent interface that is a sink for PDs. According to the model, the coherent solubility does not change under electron irradiation. It was found [36] that under electron irradiation in Zr–2.5Nb alloy precipitate-free zones form at grain boundaries. This means that the Nb segregates away from PD sinks. Using this fact in the model calculations, we can conclude that the radiation-modified incoherent solubility is higher than the coherent one, so that no large incoherent β-Nb precipitates or precipitates at grain boundaries are observed under electron irradiation.

Under cascade-producing irradiation the solubility is determined by the balance between the cascade mixing that destroys the precipitates and the radiation-enhanced diffusion that in supersaturated solutions seeks to restore precipitates. At sufficiently low temperatures cascade mixing causes β-Nb precipitates to dissolve and enrich the matrix with niobium. Further decrease of temperature slows down diffusion processes and the precipitates of ordered phase are destroyed by athermal cascade mixing. For this reason in the radiation-modified phase diagram there exists a low temperature boundary for stability of large precipitates, the location of which depends on interface type and dose rate. Above this boundary large precipitates coarsen with radiation-enhanced rate.

In this paper in order to evaluate the effect of cascade mixing on precipitate stability we considered the case of spherical precipitates. In real situation the efficiency of cascade-induced dissolution depends on precipitate shape. An example was presented in Ref. [51] showing that distributions of solute atoms after direct impingement of a single cascade onto a platelet and a spherical precipitate is quite different. The dissolution process can be much more efficient in the case of the disk-shaped or needle-like precipitates. This means that the location of low temperature threshold depends on precipitate morphology.

Let us examine in more detail the evolution of phase microstructure of alloy close to the low temperature threshold for coherent precipitate stability. Suppose that the aged alloy is subjected to cascade-producing irradiation in the temperature range near T_{coh}. Due to partial or complete cascade-induced shrinkage of preexisting precipitates the concentration of solute monomers increases and tends to $C^{\mathrm{irr}}_{\mathrm{A\,coh}}$ that is higher than the thermal equilibrium solubility $C^{\mathrm{e}}_{\mathrm{A}}$. This immediately gives rise to nucleation of coherent precipitates. However, such a newly appeared precipitate cannot grow to a size larger than the cascade size, because with a high probability it can be destroyed by a single cascade. These processes result in the formation of a steady-state size distribution of small coherent precipitate. Small precipitates, continuously nucleating and decaying under irradiation, are similar to the equilibrium heterophase fluctuations [52]. In the paper we did not take into account heterophase fluctuations. This is formally valid only at high values of interface energy [53], $\sigma \gg k_{\mathrm{B}}T(C^{\mathrm{P}}_{\mathrm{A}}/\omega)^{2/3}$, where ω is the atomic volume. The reason is that system does not want to increase its energy by creating new interfaces between second phase clusters and the matrix. In this approximation $C^{\mathrm{e}}_{\mathrm{A}}$, $C^{\mathrm{irr}}_{\mathrm{A\,coh}}$ and $C^{\mathrm{irr}}_{\mathrm{A\,inc}}$ are the equilibrium concentrations of mobile monomers $C^{\mathrm{e}}_{\mathrm{A1}}$, $C^{\mathrm{irr}}_{\mathrm{A1\,coh}}$ and $C^{\mathrm{irr}}_{\mathrm{A1\,inc}}$, which generally do not coincide with the thermal and radiation-modified solubilities, correspondingly. The solubility is defined as the total content of A-atoms in the saturated solution (with the infinite critical radius) including A-atoms in undercritical second-phase clusters that form and decay due to fluctuations, i.e.:

$$C^{\mathrm{e}}_{\mathrm{A}} = C^{\mathrm{e}}_{\mathrm{A1}} + \omega \sum_{n=2}^{\infty} n f^{\mathrm{e}}(n),$$

$$C^{\mathrm{irr}}_{\mathrm{A\,coh}} = C^{\mathrm{irr}}_{\mathrm{A1\,coh}} + \omega \sum_{n=2}^{\infty} n f(n), \tag{36}$$

where n is the number of A-atoms in the cluster, $f^{\mathrm{e}}(n)$ and $f(n)$ are the distribution functions of heterophase fluctuations without and under irradiation respectively.

The way to consider the kinetics of heterophase fluctuations under irradiation was formulated in Ref.

[53]. The nucleation of precipitates smaller than the cascade size or of the similar size we described in the framework of the theory of homogeneous nucleation. For the sake of simplicity, we ignored other mechanisms of nucleation such as the nucleation in the cascade region [54,55] or the nucleation at the site of cascade-destroyed precipitate. We have found that the fraction of small-sized particles increases drastically with decreasing interfacial energy. The fraction of solute atoms in the form of unstable precipitate can be larger than the fraction of monomers. This effect is especially important for coherent precipitates that have low interface energy.

We have noticed that the interval of operating temperatures of thermal reactors is located between low temperature thresholds for stability of coherent and incoherent precipitates of the β-Nb phase. Under these conditions a steady state, or more accurately, quasi-steady-state distribution of fine-grained β-Nb precipitates may form in the α-Zr phase supersaturated with Nb. The mechanism is connected with competition of the nucleation of coherent precipitates in a supersaturated solid solution and the dissolution of large precipitates that lose coherency upon reaching some critical size (Fig. 8).

A somewhat similar effect has been observed in the Ni–12.8at.%Al alloy during aging under irradiation with Ni^+ ions of solution annealed and quenched specimens [56,57]. In Ni–Al alloys the oversized Al segregates away from PD sinks [1]. Irradiation does not prevent nucleation and subsequent growth of coherent precipitates in regions removed from sinks. At low dose small coherent γ′-precipitates form throughout the solid solution matrix except in close proximity to interstitial dislocation loops and other defect sinks. As the dislocation loops grow with increasing dose, the precipitate-free zones enclosing the loops grow correspondingly by dissolution of the precipitates because of segregation of the oversized Al away from loops. The coherent precipitates in the sink-free regions between precipitate-free zones coarsen at a radiation-enhanced rate with the usual dependence of the mean precipitate radius on time $R \propto t^{1/3}$. At higher doses (>15 dpa at 550 °C) coherent γ′-precipitates renucleate within the precipitate-free zones in colonies, presumably in regions sufficiently removed from the dislocation loop perimeters. Obviously, reprecipitation results from the local enhancement of the Al supersaturation due to precipitate dissolution in the Al depleted zones surrounding sinks. The renucleation process leads to a decrease of the mean precipitate radius that during prolonged irradiation tends to the constant value $R = 5$ nm [56] ($T = 550$ °C). In the Ni–Al case the precipitates lost stability and behaved similar to incoherent precipitates when they became trapped into zones near sinks depleted with Al. This example shows also the importance of interaction between precipitates and other elements of the microstructure.

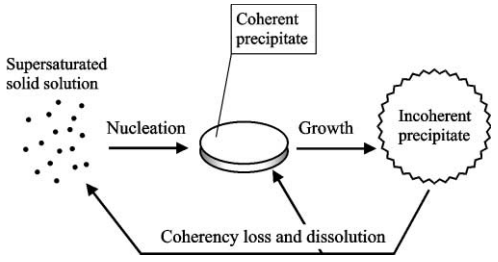

Fig. 8. Schematic illustration of formation of steady-state distribution of coherent/semi-coherent β-Nb precipitates in the α-Zr phase supersaturated with Nb.

Small coherent precipitates can suppress radiation growth and creep of Zr–Nb alloys. The point is that coherent precipitates can absorb PD, thereby decreasing the rate of processes controlled by diffusion and concentration of PD. The mechanism of defect absorption is the enhanced recombination inside coherent precipitates [10]. This mechanism is operative under special conditions, which we summarize below. Across the coherent interface, the atomic planes are continuous. This means that the perfect coherent boundary does not contain defect sites or traps, which could serve as a sink for PD. For this reason PD easily cross the coherent boundary. Since formation and migration energies of PD inside the precipitate differ from those in the matrix, the rate of mutual annihilation of vacancies and interstitials differs too. The coherent precipitate absorbs PD if the formation energy of the Frenkel pair in the matrix is greater than that in the precipitate. At a negative misfit between lattices of the precipitate and the matrix the probability of absorption of Frenkel pairs increases. The efficiency of the recombination mechanism of PD absorption by coherent precipitates at a fixed volume fraction of precipitates increases with decreasing the average size of precipitates [10].

As an experimental evidence of influence of β-Nb precipitates on radiation growth we would like to cite Ref. [39]. It was found that thermally aged Zr–Nb alloys containing high density of β-Nb precipitates exhibit an enhanced resistance to radiation growth [39]. This effect is more pronounced in the Zr–2.5Nb alloy as compared to the Zr–1.0Nb alloy. The difference is that in the Zr–2.5Nb alloy the density of β-Nb precipitates was higher than that in the Zr–1.0Nb alloy. It appears that the second phase precipitates intensify the recombination of PD created by the irradiation.

According to experimental observations, the corrosion response of Zr–2.5Nb pressure tubes improves with irradiation and correlates with the β-Nb precipitation in the α-Zr phase [34]. Measurements of irradiated Zr–2.5Nb pressure tubes show that the lattice parameter changes have usually saturate (equilibrium is reached)

by fluence of about 1×10^{25} n/m^2 [34] and can be attributed to the precipitation of Nb from supersaturated solid solution in the α-Zr phase. One could speculate that formation of the phase microstructure with slowly varying parameters is one of the important factors that provides high corrosion-resistance and service properties of Zr–Nb alloys under irradiation.

Although we did not consider evolution of the β-Zr phase, using our model we can propose an explanation of relatively high stability of grains of the β-Zr phase under irradiation at temperatures between 520 and 570 K [33,34]. According to the equilibrium phase diagram, the β-Zr phase is unstable below monotectoid temperature. Since irradiation enhances diffusion kinetics one may expect dissolution of the β-Zr phase under irradiation due to Nb loss into the matrix accompanied by lattice transformation. Moreover, under neutron irradiation cascades mixing should assist the dissolution of β-Zr phase. The following logic may help to resolve the paradox. If we assume that Nb segregate away from interfaces between the α- and β-Zr phases this would explain the stability of large grains of β-Zr phase. Indeed, migration of Nb from interfaces inside the grain interior keeps the Nb trapped in the β-Zr phase. One could argue that cascades mixing should throw away Nb atoms from the β-Zr phase into the surrounding α-Zr phase, because the β-Zr phase is enriched with Nb as compared with the α-Zr phase. However the radiation-induced segregation creates Nb denuded zones on both sides of the α/β interface. If the thickness of these zones is larger than the cascade size then the efficiency of the cascade mixing, i.e. the cascade-driven transfer of Nb atoms across the interface is very small, because of a low concentration of Nb near the interface.

5. Conclusions

- The model accounting for phase stability alteration under irradiation was described. Under irradiation the stability criteria for coherent and incoherent precipitates differ. The non-equilibrium radiation-modified phase diagram of Zr–Nb alloy was constructed, which represents conveniently the stability fields of coherent and incoherent precipitates.
- Athermal cascade-induced mixing results in appearance of the low temperature threshold for stability of precipitates larger than the mean cascade size.
- Above this threshold large precipitates undergo the Ostwald ripening with radiation-enhanced rate. Below it the alloy is maintained in a quasi-steady-state of supersaturated solid solution in dynamic equilibrium with a population of fine-grained precipitates, which nucleate continuously and grow until destruction by cascades.
- The radiation-modified phase diagram of Zr–Nb alloy shows that under in-reactor conditions incoherent β-Nb precipitates are unstable, while coherent precipitates remain stable.
- The competition between processes of cascade destruction; nucleation and growth of coherent precipitates; and coherency loss can lead to the formation of the distribution of fine-grained precipitates with slowly varying parameters. In particular, such a distribution may form in Zr–Nb alloys under thermal reactor conditions.

Acknowledgement

This work was supported by the Science and Technology Center in Ukraine, STCU Project no. 442.

Appendix A. Precipitate growth under cascade-producing irradiation

In this section we will derive the expressions for the radiation-modified coherent and incoherent solubilities. To this end we will consider the growth of coherent and incoherent precipitates under irradiation. A few cascades cannot destroy a large precipitate, therefore the cascade-induced dissolution may be considered in the average sense, i.e. destruction of the subsurface precipitate layer is assumed to result in (i) the precipitate dissolution to a depth l_1 and (ii) the formation of a shell, of inner and outer radii R and $R + l$, enriched in solute (R is the precipitate radius). Obviously, l_1 and l do not exceed the cascade size (Fig. 1). The growth rate of the precipitate volume is given by

$$4\pi R^2 \frac{\mathrm{d}R}{\mathrm{d}t} = \frac{J_\mathrm{A}}{C_\mathrm{A}^\mathrm{P} - C_\mathrm{A}|_{r=R}} - 4\pi R^2 l_1 \gamma K, \tag{A.1}$$

J_A is the total solute flux to the precipitate, $C_\mathrm{A}|_{r=R}$ is the solute concentration at the precipitate boundary, γ is the number of replacements per Frenkel pair survived the cascade relaxation (the efficiency of atomic mixing). The first term in Eq. (A.1) describes the diffusion growth/dissolution of the precipitate, whereas the second term is responsible for the cascade dissolution.

The integral over the volume occupied by the solute source $g(r)$ around the precipitate equals the number of solute atoms ejected by cascades from the precipitate

$$4\pi \int_R^{R+l} g(r) r^2 \,\mathrm{d}r = 4\pi R^2 l_1 \gamma K (C_\mathrm{A}^\mathrm{P} - C_\mathrm{A}|_{r=R}). \tag{A.2}$$

To find the solute flux J_A we use a method of influence regions [31] (see also [58]). Eqs. (1)–(5) are solved in a sink-free region enclosing the chosen precipitate. The external radius of the influence region, R_inf, is of order of the average sink spacing. Beyond this region the real

system is replaced by a homogeneous effective lossy medium.

We need boundary conditions for the diffusion problem. In the case of low volume fraction of sinks the major changes in the diffusant concentrations are localized within a distance of order of the sink size. Hence, at $r = R_{\text{inf}}$ the concentrations of PDs and solute, to a good accuracy, equal their average values in the effective medium

$$C_{\text{n}}|_{r \geqslant R_{\text{inf}}} = \overline{C}_{\text{n}}, \quad \text{n} = \text{A}, \text{i}, \text{v}. \tag{A.3}$$

We consider diffusion-controlled growth of precipitates and assume that the thermal equilibrium concentration of solute, C_{A}^{R}, is maintained at the precipitate boundary

$$C_{\text{A}}|_{r=R} = C_{\text{A}}^{\text{R}}, \tag{A.4}$$

which is given by the Gibbs–Thomson formula [29]

$$C_{\text{A}}^{\text{R}} = C_{\text{A}}^{\text{e}} \exp\left(\frac{1 - C_{\text{A}}^{\text{e}}}{C_{\text{A}}^{\text{P}} - C_{\text{A}}^{\text{e}}} \frac{2\sigma\omega}{k_{\text{B}} TR}\right), \tag{A.5}$$

where C_{A}^{e} is the thermal solubility of the solute.

The form of boundary conditions for PD at the precipitate boundary depends essentially on the structure of precipitate-matrix interface, therefore coherent and incoherent precipitates will be considered separately.

A.1. Coherent precipitate

The perfect coherent interface is transparent to PDs because it is free of defect sites and does not absorb vacancies and interstitials. For this reason in the vicinity of the isolated coherent precipitate situated far from sinks the PD fluxes are small compared to the solute flux and practically do not influence the growth of the coherent precipitate. In the approximation of a low volume fraction of sinks (i.e. neglecting diffusion interaction between the chosen precipitate and sinks) the concentration profiles of diffusants near the coherent precipitate are defined by equations

$$\mathbf{j}_{\text{i}} = \mathbf{j}_{\text{v}} = 0, \tag{A.6}$$

$$\text{div}\,\mathbf{j}_{\text{A}} = g(r), \tag{A.7}$$

with boundary conditions (A.3) and (A.4).

Solution to this boundary problem is similar to that presented in the Ref. [14]. Eq. (A.6) yields

$$D_{\text{i}} C_{\text{i}} = \overline{D}_{\text{i}} \overline{C}_{\text{i}}, \quad C_{\text{v}}/D_{\text{v}} = \overline{C}_{\text{v}}/\overline{D}_{\text{v}}. \tag{A.8}$$

Using these, we rewrite $\mathbf{j}_{\text{A}}$ inside the influence region in the form

$$\mathbf{j}_{\text{A}} = -\left(\frac{d_{\text{Av}} d_{\text{Bv}} C_{\text{v}}}{D_{\text{v}}} + \frac{\lambda D_{\text{i}} C_{\text{i}}}{(C_{\text{B}} + \lambda C_{\text{A}})^2}\right) \nabla C_{\text{A}}. \tag{A.9}$$

From the solution of the diffusion problem given by Eqs. (A.3)–(A.9) we can obtain the total solute flux to the boundary of the coherent precipitate

$$J_{\text{A}} = 4\pi R D_{\text{A coh}}^{\text{irr}} (\overline{C}_{\text{A}} - C_{\text{A}}^{\text{R}}) + 4\pi R \int_R^{R+l} r g(r)\, \text{d}r, \tag{A.10}$$

where the coefficient of interdiffusion, $D_{\text{A coh}}^{\text{irr}}$, given by Eq. (14) is the same as that in the case of cascade-free irradiation [14].

Substituting Eq. (A.10) into Eq. (A.1) we obtain the growth rate of the coherent precipitate

$$\frac{\text{d}R}{\text{d}t} = \frac{D_{\text{A coh}}^{\text{irr}}}{R(C_{\text{A}}^{\text{P}} - C_{\text{A}}^{\text{R}})} \left\{ \overline{C}_{\text{A}} - C_{\text{A}}^{\text{R}} - \frac{1}{D_{\text{A coh}}^{\text{irr}}} \int_R^{R+l} g(r) \left(\frac{r^2}{R} - r\right) \text{d}r \right\}. \tag{A.11}$$

It is seen that the cascade dissolution is described by the negative term which contribution increases with temperature decreasing. As distinct from the case of cascade-free irradiation ($g(r) = 0$), the cascade-producing irradiation changes the condition for the coherent precipitate to be in equilibrium with the solid solution.

The average solute concentration at which $\text{d}R/\text{d}t = 0$ is an analog of the thermal solute solubility. It plays the role of the radiation-modified solute solubility with respect to coherent precipitates, $C_{\text{A coh}}^{\text{irr}}$. To the lowest order in the small parameter l/R, i.e. for precipitates larger than the cascade size, $C_{\text{A coh}}^{\text{irr}}$ is written as

$$C_{\text{A coh}}^{\text{irr}} = \lim_{R \to \infty} \left(C_{\text{A}}^{\text{R}} + \frac{1}{D_{\text{A coh}}^{\text{irr}}} \int_R^{R+l} g(r) \left(\frac{r^2}{R} - r\right) \text{d}r \right) = C_{\text{A}}^{\text{e}} + \frac{D_{\text{mix}}}{D_{\text{A coh}}^{\text{irr}}} (C_{\text{A}}^{\text{P}} - C_{\text{A}}^{\text{e}}), \tag{A.12}$$

where $D_{\text{mix}} = 0.5 l_1 l \gamma K \cong 0.5 l^2 \gamma K \equiv d_{\text{mix}} K$ is the diffusion coefficient due to cascade mixing. The parameters of cascade mixing are combined to form the mixing efficiency, d_{mix}, which is used in calculations as an adjustable parameter.

Though relation (A.12) is the equation for the unknown $C_{\text{A coh}}^{\text{irr}}$ (because $D_{\text{A coh}}^{\text{irr}}$ depends on $C_{\text{A coh}}^{\text{irr}}$), it nevertheless shows that the cascade dissolution is equivalent to an increase in the solute solubility. If we neglect the dependence of $D_{\text{A coh}}^{\text{irr}}$ on alloy composition, then Eq. (A.12) is reduced to that derived in Refs. [27,28] within the framework of one-component model.

A.2. Incoherent precipitate

Here we will find the growth rate and the stability condition of incoherent precipitates. In contrast to the coherent precipitate, the boundary of the incoherent one, similarly to grain boundaries, is a good sink for PDs, therefore, in the diffusion-controlled case the

thermal equilibrium concentrations of vacancies and interstitials are maintained at it.

$$C_v|_{r=R} = C_v^e, \quad C_i|_{r=R} = 0. \tag{A.13}$$

Neglecting recombination of PD inside the influence region (recombination is taken into account when finding the average PD concentrations), i.e. assuming that the recombination length $L_R \sim a/(4\pi C_v)^{1/2} \gg R$, where a is the mean atomic spacing, from Eqs. (1)–(5) we obtain the diffusion problem for the quasy-steady concentration profiles in the vicinity of the incoherent precipitate.

$$\operatorname{div} \mathbf{j}_n = K, \quad n = i, v, \tag{A.14}$$

$$\operatorname{div} \mathbf{j}_A = g(r). \tag{A.15}$$

To define the radius of the influence region, R_{inf}, we use the following considerations. If all sinks are distributed in the matrix homogeneously, then there exists a surface separating sinks, at which PD fluxes vanish, $\mathbf{j}_{i,v}|_S = 0$. After averaging over all possible positions of all other sinks except the chosen incoherent precipitate, the separating surface of a complicated shape transforms into the sphere, at which the relation $\mathbf{j}_{i,v}|_{r=R_{inf}} = 0$ still holds. The latter is not an additional boundary condition for Eqs. (A.14), but the relation that makes the choice of R_{inf} unique. Since all PD created by irradiation inside the influence region cannot escape it ($\mathbf{j}_{i,v}|_{r=R_{inf}} = 0$), the total fluxes of vacancies and interstitials to the precipitate equal, $J_v = J_i$, provided that R_{inf} is the same for vacancies and interstitials. Generally speaking, R_{inf} depends on PD type. This should be taken into account when considering bias effects. For the problem addressed here bias effects are not essential, since amount of segregation is controlled by the values of J_i and J_v, rather than by their small difference. Upon integrating Eqs. (A.14) and (A.15) we obtain

$$\frac{\mathrm{d}D_i C_i}{\mathrm{d}r} = \frac{J_i}{4\pi r^2}\left(1 - \frac{r^3 - R^3}{R_{inf}^3 - R^3}\right), \tag{A.16}$$

$$d_{Bv}\frac{\mathrm{d}C_v}{\mathrm{d}r} - (d_{Av} - d_{Bv})C_v^2\frac{\mathrm{d}}{\mathrm{d}r}\frac{C_A}{C_v} = \frac{J_v}{4\pi r^2}\left(1 - \frac{r^3 - R^3}{R_{inf}^3 - R^3}\right), \tag{A.17}$$

$$d_{Av}C_v^2\frac{\mathrm{d}}{\mathrm{d}r}\frac{C_A}{C_v} + \frac{\mathrm{d}}{\mathrm{d}r}\frac{\lambda C_A D_i C_i}{C_B + \lambda C_A} = \frac{J_A}{4\pi r^2} - \frac{1}{r^2}\int_R^r r'^2 g(r')\,\mathrm{d}r', \tag{A.18}$$

where $J_{A,i,v}$ are the total fluxes to the precipitate. The solution of Eq. (A.16) is given by

$$D_i C_i = \frac{J_i}{4\pi R} f(r),$$
$$f(r) = \int_R^r \left(1 - \frac{r^3 - R^3}{R_{inf}^3 - R^3}\right)\frac{R\mathrm{d}r}{r^2}, \tag{A.19}$$

$$J_i = 4\pi R \overline{D}_i \overline{C}_i (f(R_{inf}))^{-1} \approx 4\pi R \overline{D}_i \overline{C}_i. \tag{A.20}$$

To the lowest order in volume fraction of sinks, $R/R_{inf} \ll 1$, we obtain from Eqs. (A.17)–(A.19)

$$d_{Av}C_v^2\frac{\mathrm{d}}{\mathrm{d}r}\frac{C_A}{C_v} + \frac{J_v}{4\pi R}\frac{\mathrm{d}}{\mathrm{d}r}\frac{\lambda C_A}{C_B + \lambda C_A}\left(1 - \frac{R}{r}\right) = \frac{J_A}{4\pi r^2} - \frac{1}{r^2}\int_R^r r'^2 g(r')\,\mathrm{d}r', \tag{A.21}$$

$$d_{Bv}(C_v - C_v^e) = \frac{J_v}{4\pi R}\left(1 - \frac{R}{r}\right)\frac{C_B + \kappa C_A}{C_B + \lambda C_A} + \frac{d_{Av} - d_{Bv}}{d_{Bv}}\left[\frac{J_A}{4\pi R}\left(1 - \frac{R}{r}\right) - \int_R^r \frac{\mathrm{d}r'}{r'^2}\int_R^{r'} \mathrm{d}r'' r''^2 g(r'')\right], \tag{A.22}$$

$$\kappa \equiv \frac{d_{Ai}d_{Bv}}{d_{Bi}d_{Av}}\xi. \tag{A.23}$$

Substituting Eq. (A.22) into Eq. (A.21) and changing the spatial variable, $x = 1 - R/r$, we derive the equation for the concentration profile of solute atoms near the incoherent precipitate

$$\left\{d_{Av}C_v^e + (\mu - 1)I(x) + \frac{J_v}{4\pi R}\left[\frac{\mu C_B + \lambda C_A}{C_B + \lambda C_A} + \frac{\lambda(C_B + \mu C_A)}{(C_B + \lambda C_A)^2} + (\mu - 1)\frac{\dot{\Omega}}{J_v}\right]\right\}\frac{\mathrm{d}C_A}{\mathrm{d}x} + \frac{J_v}{4\pi R}\frac{(\mu + \lambda)C_B C_A}{C_B + \lambda C_A} = \left(\frac{\dot{\Omega}}{4\pi R} + I_2(x)\right)(C_B + \mu C_A), \tag{A.24}$$

$$I(x) = I_1(x) + xI_2(x), \tag{A.25}$$

$$I_1 = R^2\int_0^x \frac{g(x')x'\,\mathrm{d}x'}{(1 - x')^4}, \quad I_2 = R^2\int_x^1 \frac{g(x')\,\mathrm{d}x'}{(1 - x')^4}, \tag{A.26}$$

where $\mu \equiv d_{Av}/d_{Bv}$ and $\dot{\Omega} \equiv 4\pi R^2 \dot{R}(C_A^P - C_A^R)$.

Solution of Eq. (A.24) at an arbitrary solute concentration and $\dot{R} \neq 0$ is very cumbersome. At first we will consider a simple limiting case, $d_{Av} = d_{Bv}$, $\lambda C_A \ll 1$ and $C_A \ll 1$, which admits an analytical solution with clear physical interpretation. Linearizing Eq. (A.24), we find its solution, then we subject the solution to boundary conditions (A.3) and (A.4) in order to find the uncertain constant $\dot{\Omega}$, i.e. the precipitate growth rate

$$4\pi R^2\frac{\mathrm{d}R}{\mathrm{d}t} = \frac{J_v}{C_A^P - C_A^R}\frac{\lambda - 1}{1 - \varphi}(\overline{C}_A - C_{A\,inc}^{irr}(R)), \tag{A.27}$$

$$J_v = 4\pi R d_{Av}(\overline{C}_v - C_v^e), \tag{A.28}$$

$$\varphi = \left[1 + \left(\frac{\overline{C}_v}{C_v^e} - 1\right)(\lambda + 1)\right]^{(1-\lambda)/(1+\lambda)}, \tag{A.29}$$

$$C_{A\,inc}^{irr}(R) = \varphi\left\{C_A^R + \frac{R^2}{d_{Av}(\overline{C}_v - C_v^e)(\lambda - 1)} \times \int_0^{l/R}\left[\left[1 + \left(\frac{\overline{C}_v}{C_v^e} - 1\right)(\lambda + 1)x\right]^{(1-\lambda)/(1+\lambda)} - 1\right]\frac{g(x)\,dx}{(1-x)^4}\right\}. \tag{A.30}$$

It follows from Eq. (A.27) that $C_{A\,inc}^{irr}(R)$ is the radiation-modified incoherent solubility. In the case of a large precipitate, which corresponds to the lowest order in the ratio l/R, the radiation-modified incoherent solubility is given by

$$C_{A\,inc}^{irr} = \lim_{R\to\infty}(C_{A\,inc}^{irr}(R)) = \varphi\left[C_A^e + \frac{D_{mix}}{d_{Av}C_v^e}(C_A^P - C_A^e)\right]. \tag{A.31}$$

Here the multiple φ accounts for the influence of radiation-induced segregation on the precipitate growth. It coincides with that derived for cascade-free irradiation [13]. At $\lambda > 1$ solute atoms migrate to sinks. Consequently, segregation results in a reduction of solubility, since, according to Eq. (A.29), $\varphi < 1$. On the contrary, due to cascade mixing described by the term $D_{mix}(C_A^P - C_A^e)/d_{Av}C_v^e$, the solubility increases. At $\lambda < 1$ both segregation and mixing shift the solubility limit to higher concentrations. This means that even in a supersaturated solid solution (at $\overline{C}_A > C_A^e$) the incoherent precipitates may become unstable when $\overline{C}_A < C_{A\,inc}^{irr}$ (see Eq. (A.27)).

Let us find $C_{A\,inc}^{irr}$ in a general case. For this purpose in Eq. (A.24) we set $\dot{\Omega} = \dot{R} = 0$. The whole region of variation of x is divided into two subregions, namely, the region of action of the cascade source, $0 \leqslant x \leqslant l/(R + l) \equiv \varepsilon$, and the diffusion region, $\varepsilon \leqslant x \leqslant 1$. In the diffusion region the solution of Eq. (A.24) correct to the first order in the small parameter ε is written as

$$x = \frac{4\pi R d_{Bv}\widetilde{C}_v^e(C_B + \lambda C_A)}{J_v(\kappa + 1)}\left[\left(\frac{\widetilde{C}_B C_A}{\widetilde{C}_A C_B}\right)^{(1+\kappa)/(1-\kappa)} - 1\right], \tag{A.32}$$

where $\widetilde{C}_v^e$ is given by Eq. (13). $\widetilde{C}_{B,A} = C_{B,A}(\varepsilon)$ are the values of concentrations at the outer boundary of the cascade source $x = \varepsilon$, which are determined from the solution in the region $0 \leqslant x \leqslant \varepsilon$,

$$C_A(x) = C_A^e + \frac{D_{mix}}{D_{A\,inc}^{irr}}(C_A^P - C_A^e)\left(2\frac{x}{\varepsilon} - \left(\frac{x}{\varepsilon}\right)^2\right), \tag{A.33}$$

where $D_{A\,inc}^{irr}$ is given by Eq. (15).

At $x \to 1$ the solute concentration tends to the average value, which is the radiation-modified solubility, $C_{A\,inc}^{irr}$, that we are looking for. Setting $x = 1$ and using Eq. (A.22), Eq. (A.32) can be transformed into the form

$$\frac{C_{A\,inc}^{irr}}{1 - C_{A\,inc}^{irr}} = \frac{\widetilde{C}_A}{1 - \widetilde{C}_A}\left[1 + \left(\frac{\overline{C}_v}{\widetilde{C}_v^e} - 1\right) \times \frac{1 + \kappa}{1 + (\kappa - 1)C_{A\,inc}^{irr}}\right]^{(1-\kappa)/(1+\kappa)}. \tag{A.34}$$

Note that $\widetilde{C}_A \to C_A^e$ and $\widetilde{C}_v \to C_v^e$ at $d_{mix} \to 0$, i.e. Eq. (A.34) reduces to the relation

$$\frac{C_{A\,inc}^{irr}}{1 - C_{A\,inc}^{irr}} = \frac{C_A^e}{1 - C_A^e}\left[1 + \left(\frac{\overline{C}_v}{C_v^e} - 1\right) \times \frac{1 + \kappa}{1 + (\kappa - 1)C_{A\,inc}^{irr}}\right]^{(1-\kappa)/(1+\kappa)}, \tag{A.35}$$

which was obtained in Ref. [14] for the case of cascade-free irradiation. Thus, the cascade disordering of precipitates is formally equivalent to a renormalization of boundary concentrations. In the limiting case $d_{Av} = d_{Bv}$ and $C_A \ll 1$, from Eq. (A.34) we again obtain Eq. (A.31).

The results of this section are valid also for coherent precipitates associated with PD sinks. The difference is that vacancies and interstitial atoms arriving to the precipitate recombine not at the precipitate–matrix interface, but at the PD sink which is situated inside this precipitate.

References

[1] F.V. Nolfi (Ed.), Phase Transformation during Irradiation, Applied Science, London, 1983.
[2] G. Martin, P. Bellon, F. Soisson, in: W.C. Johnson, J.M. Howe, B.E. Laughlin, W.A. Sofa (Eds.), Solid to Solid Phase Transformations, Minerals, Metals and Materials Society, Pittsburgh, PA, 1994, p. 937.
[3] H. Wollenberger, J. Nucl. Mater. 216 (1994) 63.
[4] K.C. Russell, J. Nucl. Mater. 206 (1993) 129.
[5] G. Szenes (Ed.), Physics of Irradiation Effects in Metals, Mater. Sci. Forum. 97–99 (1992).
[6] V. Naundorf, Int. J. Mod. Ph. B 6 (1992) 2925.
[7] A.A. Turkin, C. Abromeit, V. Naundorf, Diff. Defect Data–Solid State Data 143–147 (1997) 521.
[8] A.D. Marwick, J. Phys. F 8 (1978) 1849.
[9] G. Martin, Phys. Rev. B 21 (1980) 2122.
[10] A.A. Turkin, A.S. Bakai, J. Nucl. Mater. 270 (1999) 349.
[11] C. Abromeit, V. Naundorf, H. Wollenberger, J. Nucl. Mater. 155–157 (1988) 1174.
[12] U. Scheuer, Radiat. Eff. 105 (1987) 85.
[13] A.S. Bakai, A.A. Turkin, J. Nucl. Mater. 152 (1988) 331.
[14] A.S. Bakai, A.A. Turkin, in: R.E. Stoller, A.S. Kumar, D.S. Gelles (Eds.), Effects of Radiation on Materials: 15th

International Symposium, vol. I, ASTM STP 1125, American Society for Testing and Materials, Philadelphia, PA, 1992, p. 709.
[15] A.A. Turkin, A.S. Bakai, A.V. Buts, Mater. Sci. Forum 97–99 (1992) 343.
[16] W.G. Wolfer, J. Nucl. Mater. 114 (1983) 292.
[17] A.B. Lidiard, Acta Metall. 34 (1986) 1487.
[18] S.M. Murphy, Philos. Mag. A 58 (1988) 417.
[19] H. Wiedersich, P.R. Okamoto, N.Q. Lam, J. Nucl. Mater. 83 (1979) 98.
[20] A.D. Marwick, J. Nucl. Mater. 135 (1985) 68.
[21] N. Nastasi, J.W. Mayer, Mater. Sci. Eng. R 12 (1994) 1.
[22] Y.-T. Cheng, Mater. Sci. Rep. 5 (1990) 47.
[23] R.S. Averback, J. Nucl. Mater. 216 (1994) 49.
[24] D.J. Bacon, T. Diaz de la Rubia, J. Nucl. Mater. 216 (1994) 275.
[25] T. Diaz de la Rubia, R.S. Averback, H. Hsieh, R. Benedek, J. Mater. Res. 4 (1989) 579.
[26] G. Gleiter, in: R.W. Cahn, P. Haasen (Eds.), Physical Metallurgy (Part 1), North Holland Physics, Amsterdam, 1983, p. 110.
[27] A.D. Brailsford, J. Nucl. Mater. 56 (1975) 7.
[28] A.S. Bakai, N.M. Kirukhin, Problems Atomic Sci. Technol., Ser.: Phys. Rad. Damage 5 (28) (1983) 33 (in Russian).
[29] J.W. Christian, The Theory of Transformations in Metals and Alloys. Part I: Equilibrium and General Kinetic Theory, 2nd Ed., Pergamon, 1975.
[30] A.D. Brailsford, R. Bullough, Philos. Trans. Roy. Soc. Lond. A 302 (1465) (1981) 87.
[31] V.V. Slezov, Sov. Phys. Solid State 31 (1989) 1289.
[32] A.S. Bakai, A.V. Buts, A.A. Turkin, Metallofizika 13 (1991) 68, in Russian.
[33] M. Griffiths, J.F. Mecke, J.E. Winegar, in: E.R. Bradley, G.P. Sabol (Eds.), Zirconium in the Nuclear Industry: 11th International Symposium, ASTM STP 1295, American Society for Testing and Materials, Philadelphia, PA, 1996, p. 580.
[34] V.F. Urbanic, M. Griffiths, in: D.S. Gelles, R.K. Nanstad, A.S. Kumar, E.A. Little (Eds.), Effects of Radiation on Materials: 17th International Symposium, vol. I, ASTM STP 1270, American Society for Testing and Materials, Philadelphia, PA, 1996, p. 1088.
[35] C.D. Cann, C.B. So, R.C. Styles, C.E. Coleman, J. Nucl. Mater. 205 (1993) 267.
[36] O.T. Woo, R.M. Hutcheon, C.E. Coleman, Mater. Res. Soc. Symp. Proc. 373 (1995) 189.
[37] C.E. Coleman, R.W. Gilbert, C.J.C. Carpenter, G.C. Weatherly, in: Phase Stability During Irradiation, AIME, 1981, p. 567.
[38] V. Perovic, A. Perovic, G.C. Weatherly, L.M. Brown, G.R. Purdy, R.G. Fleck, R.A. Holtl, J. Nucl. Mater. 205 (1993) 251.
[39] V.F. Zelenskii, A.I. Stukalov, I.M. Nekludov, et al., Problems Atomic Sci. Technol. Ser.: Radiation Damage Phys. Radiation Mater. Sci. N 1 (64) (1995) (in Russian).
[40] S.A. Averin, V.L. Panshenko, A.V. Kozlov, L.P. Sinelnikov, V.N. Shishov, A.V. Nikulina, in: G.P. Sabol, G.D. Moan (Eds.), Zirconium in the Nuclear Industry: 12th International Symposium, ASTM STP 1354, American Society for Testing and Materials, Philadelphia, PA, 2000. p. 105.
[41] V.V. Bryk, V.N. Voyevodin, V.F. Zelensky, I.M. Neklyudov, A.M. Parshin, in: N.M. Packan, R.E. Stoller, A.S. Kumar (Eds.), Effects of Radiation on Materials: 14th International Symposium, vol. I, ASTM STP 1046, American Society for Testing and Materials, Philadelphia, PA, 1989, p. 437.
[42] G.M. Hood, H. Zou, D. Gupta, R.J. Schultz, J. Nucl. Mater. 223 (1995) 122.
[43] G.M. Hood, H. Zou, R.J. Schultz, N. Matsuura, A.J. Roy, J.A. Jackman, Defect Diff. Forum 143–147 (1997) 49.
[44] G.M. Hood, H. Zou, R.J. Schultz, N. Matsuura, Defect Diff. Forum 143–147 (1997) 55.
[45] A.D. King, G.M. Hood, R.A. Holt, J. Nucl. Mater. 185 (1991) 174.
[46] A.S. Zaimovskii, A.V. Nikulina, N.G. Reshetnikov, Zirconium Alloys in Atomic Engineering, Energoizdat, Moscow, 1981.
[47] G.C. Weatherly, R.B. Nicholson, Philos. Mag. 17 (1968) 801.
[48] W.A. Jesser, Philos. Mag. 19 (1969) 993.
[49] L.M. Brown, G.R. Woolhaus, Philos. Mag. 21 (1970) 329.
[50] I.P. Abriata, J.C. Bolcich, Bull. Alloy Phase Diagram 3 (1982) 34.
[51] A.A. Turkin, C. Abromeit, V. Naundorf, J. Nucl. Mater. 233–237 (1996) 979.
[52] Ya.I. Frenkel, Kinetic Theory of Liquids, Oxford University, Oxford, 1946.
[53] A.A. Turkin, A.S. Bakai, A.V. Buts, in: W.C. Johnson, J.M. Howe, B.E. Laughlin, W.A. Sofa (Eds.), Solid to Solid Phase Transformations, Minerals Metals and Materials Society, Pittsburgh, PA, 1994, p. 987.
[54] A.S. Bakai, A.A. Turkin, Problems Atomic Sci. Technol., Ser.: Radiation Damage Phys. Radiation Mater. Sci. 1 (39) (1987) 12 (in Russian).
[55] A.S. Bakai, Mater. Sci. Forum 97–99 (1992) 307.
[56] D.I. Potter, D.G. Ryding, J. Nucl. Mater. 71 (1977) 14.
[57] D.I. Potter, A.W. McCormick, Acta Metall. 27 (1979) 933.
[58] A.D. Brailsford, R. Bullough, J. Nucl. Mater. 44 (1972) 121.